A MATRIX ISOLATION AND COMPUTATIONAL STUDY OF THE WATER-SULFUR HEXFLUORIDE VAN DER WAALS COMPLEX

by

Allison Leninger

A Thesis
Submitted to the
Graduate Faculty
of
George Mason University
in Partial Fulfillment of
The Requirements for the Degree
of
Master of Science
Chemistry

Committee:

_____ Dr. Paul Cooper, Thesis Director

_____ Dr. Gerald Weatherspoon, Committee Member

_____ Dr. Mikell Paige, Committee Member

_____ Dr. John Schreifels, Department Chairperson

_____ Dr. Donna M. Fox, Associate Dean, Office of Student Affairs & Special Programs, College of Science

_____ Dr. Peggy Agouris, Dean, College of Science

Date: _____ Spring Semester 2016
George Mason University
Fairfax, VA

A Matrix Isolation and Computational Study of the Water-Sulfur Hexafluoride Van Der Waals Complex

A thesis submitted in partial fulfillment of the requirements for the degree of Master of Science at George Mason University

By

Allison Leninger
Bachelor of Science
University of Mary Washington, 2013

Director: Dr. Paul Cooper
Department of Chemistry

Spring Semester 2016
George Mason University
Fairfax, VA

ACKNOWLEDGEMENTS

I would like to thank my family and friends for their continued support throughout my graduate studies. I would also like to thank Yuki for always being there to help answer my questions and assist me in my research; Dr. Cooper for his dedication and assistance throughout my research project; My committee members, Dr. Paige and Dr. Weatherspoon, who helped me edit my paper and, finally, Jolayana Wold and Jonathan Boron whose previous work helped further my own studies.

TABLE OF CONTENTS

Page

LIST OF TABLES

Table **Page**

LIST OF FIGURES

Figure **Page**

LIST OF FIGURES

Figure **Page**

ABSTRACT

A MATRIX ISOLATION AND COMPUTATIONAL STUDY OF THE WATER-SULFUR HEXAFLUORIDE VAN DER WAALS COMPLEX

Allison Leninger, M.S.

George Mason University, 2016

Thesis Director: Dr. Paul Cooper

This thesis describes the theoretical and experimental studies of the H_2O-SF_6 Van der Waals complex as well as the H_2O-NF_3 complex. Both SF_6 and NF_3 are extremely potent greenhouse gases and therefore cause significant concern when released into the atmosphere as industrial waste. Until recently the actual atmospheric burden of these two gases was not fully understood when better atmospheric modeling suggested that they have a larger impact on the rising global temperatures than once believed. Additionally, complexation with abundant water molecules in the atmosphere causes the wavelengths at which these molecules absorb infrared radiation to change, making it impossible to accurately model the global climate without taking this fact into account. Therefore, presented here is an in depth investigation into the water molecule interactions of both SF_6 and NF_3 in an effort to better understand the impact of these greenhouse gas pollutants on our planet.

INTRODUCTION
Part I: Global warming and its Causes

The rising temperatures on planet Earth have become a more significant cause for concern over the past few decades. Some people present the argument that global warming is a normal process caused by natural changes in the environment. One of the key origins of this type of argument rests on the fact that the most abundant greenhouse gas in our atmosphere is water. The amount of water vapor present in the air at a given time is largely affected by the temperature of the air and the humidity levels. On average, the atmosphere is comprised of approximately 2-3% water vapor while CO_2 comprises only 0.04%.[1] However, 97% of climate scientists agree that the warming trends we have observed over the course of this past century are due to human activities, which release numerous different types of greenhouse gases into our atmosphere. [2]

Greenhouse gases (GHG) allow direct, shortwave energy from the sun to pass through the atmosphere and hit Earth's surface. Once that energy is reradiated in the atmosphere as infrared, longer-wave energy, it is absorbed by the GHG compounds, preventing its escape into space and trapping it in the lower atmosphere. [3] Under normal conditions this effect, known as the greenhouse gas effect, is what allows the planet to maintain a temperature that can sustain life. Without the greenhouse effect the surface

temperature of the Earth would be approximately -21°C causing all water on the surface to freeze thereby making Earth uninhabitable.

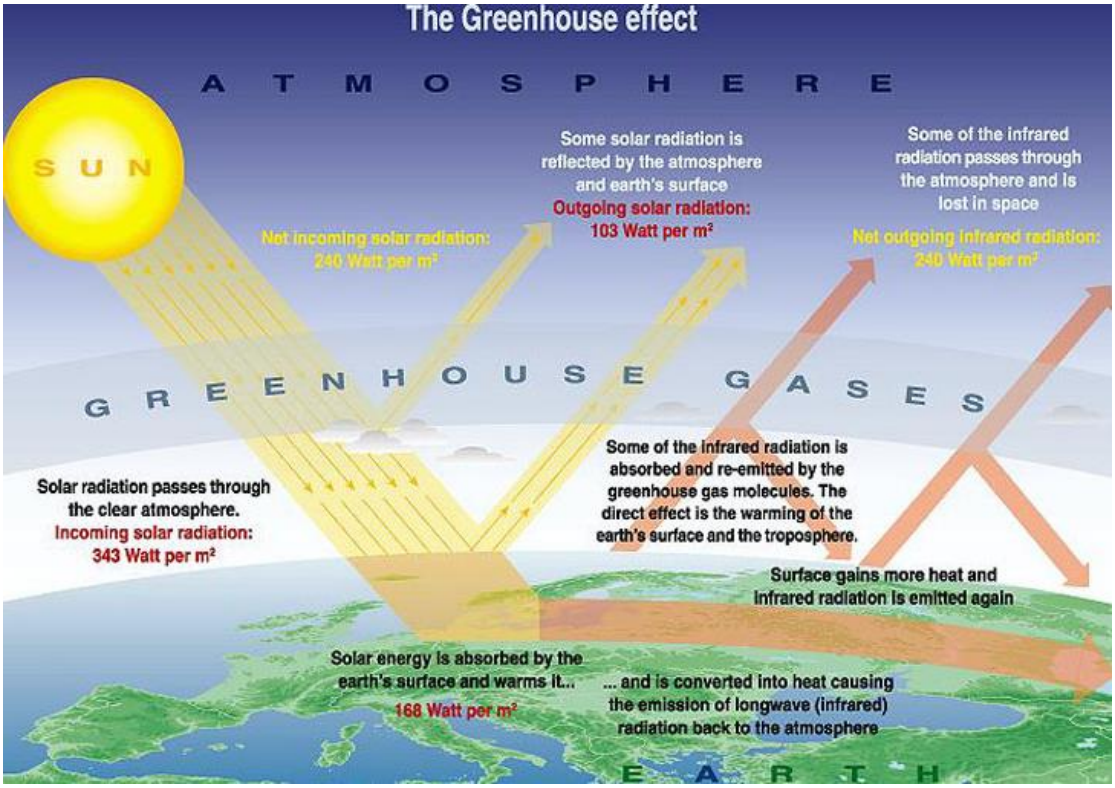

Figure 1: The Greenhouse Effect[4]

There are three major factors that influence the greenhouse effect and the temperature of the Earth: the total energy influx from the sun, which is a factor both solar activity and Earth's distance from the sun, the composition of the atmosphere, and the ability of Earth's surface to reflect light back into space, albedo. The only thing that has changed in recent history is the composition of gases in our atmosphere. The presence of

these gases in the atmosphere is regulated by various natural processes. Plant uptake of CO_2 during photosynthesis and CO_2 dissolution into the oceans are both major carbon sinks that help to buffer the GHG effect and slow warming of the atmosphere.

There are numerous natural, as well as anthropogenic sourced gases that absorb infrared radiation in this region and the overwhelming rate at which humans are contributing GHG such as CO_2, CH_4, chlorofluorocarbons (CFCs), hydrofluorocarbons (HFCs), and perfluorocarbons (PFCs), as well as sulfur hexafluoride (SF_6), is the leading cause of this unprecedented warming trend as shown below. [3]

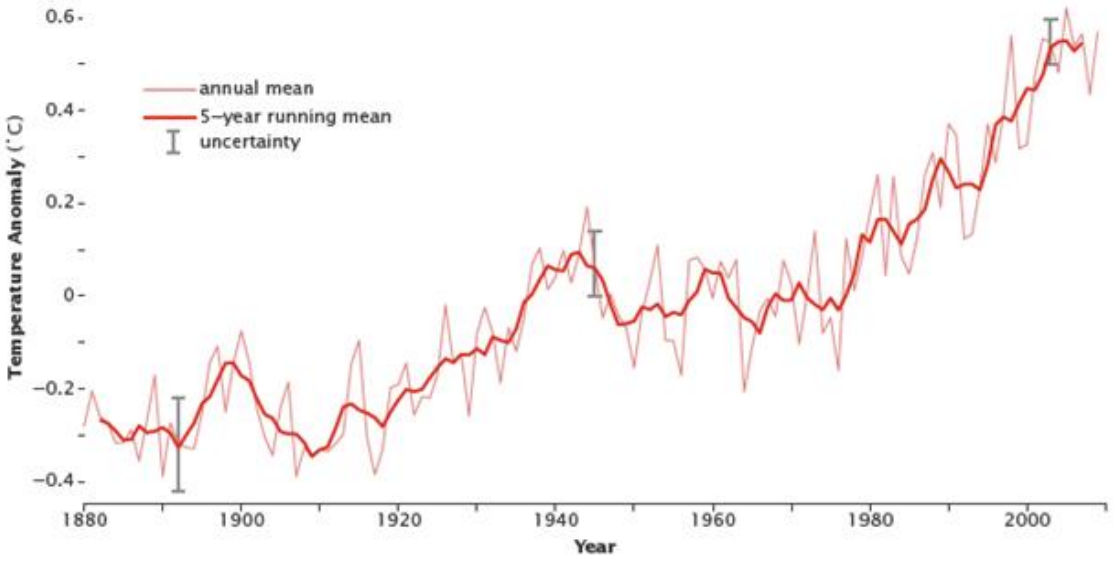

Figure 2: Global Mean Surface Temperature Over Time[4]

Table 1: GHG global warming potentials[5]

Greenhouse gas	**Global Warming Potential (GWP) over 100 years**	**% of total anthropogenic GHG emissions (2010)**
Carbon dioxide	1	76%
Methane (CH_4)	25	16%
Nitrous oxide (N_2O)	298	6%
Hydrofluorocarbons (HFCs)	124-14,800	< 2%
Perfluorocarbons (PFCs)	7,390-12,200	< 2%
Sulfur hexafluoride (SF_6)	22,800	< 2%
Nitrogen trifluoride (NF_3)	17,200	< 2%

The natural sinks that normally keep GHGs in check cannot keep up with the overwhelming amount of anthropogenic GHG being emitted into the atmosphere. Not to mention many of the afore mentioned anthropogenic gases do not have natural sinks in the environment and are only destroyed very slowly through atmospheric chemical reactions. CO_2 is a natural and anthropogenic sourced GHG. Since the industrial revolution, when human activity began to introduce CO_2 into the atmosphere at a much faster rate, the world's oceans have stored nearly half of the carbon from CO_2 emission. [2] However, due to the acidic nature of CO_2, which forms carbonic acid upon dissolution in water, the large amounts of stored CO_2 is beginning to decrease the overall pH of ocean

water and is having a negative impact on marine life. Additionally, higher temperatures will lead to rise in sea levels, warming oceans, and in increase in extreme weather events.

It is obvious that something has to be done about global warming, but addressing this problem is difficult because there is not one thing or one nation that can be blamed. There are numerous causes of this problem that need to be addressed. For example, CO_2 is the most commonly blamed culprit in global warming arguments but other GHGs present in the atmosphere can have an even more detrimental effect despite being overwhelmingly dominated by CO_2 in terms of atmospheric tonnage. Other anthropogenic GHGs such as CFCs and sulfur hexafluoride have global warming potentials (Table 1) thousands of times greater than CO_2. Therefore, these types of gases with high global warming potentials should also be addressed. In this paper, two such gases that are studied are NF_3 and SF_6.

INTRODUCTION
Part II: SF_6 and NF_3

Sulfur hexafluoride is a chemically inert, colorless, odorless gas that has extremely high insulating capacities. The high electron affinity of the molecule allows for the capture of free electrons. Once the free electrons are captured, the large, heavy ions formed by SF_6 have such low mobility that they effectively prevent electron avalanches. The SF_6 gas is resistant to this breakdown process; preventing electron avalanches is essential in order to avoid the breakdown of the insulating gas. Dielectric materials are electrical insulators that can be polarized by an electric field. The dielectric strength of an insulating gas is measured by its ability to resist breakdown upon application of a strong electrical field. The dielectric properties of SF_6, which are about 2.5 times that of air under the same conditions, combined with its chemical inertness allow it to act as an excellent insulator for electrical applications. [6]

As a result of these unique properties, SF_6 is primarily used as a dielectric medium within voltage breakers, switchgears and various other electrical equipment within the electrical industry. Industrial usage of SF_6 began around 1953 and since then the production has grown steadily along with increasing demand. However it was not until 1972, when insulated switchgear became more widespread, along with the eventual

ban of polychlorinated biphenyls in the United States, did the production pick up to an even greater rate. [7]

Prior to the use of SF_6, polychlorinated biphenyls (PCBs) were the main electrical insulators used in the industry since they have many of the desirable characteristics which were discussed previously. However, in 1979 PCBs were banned due to suggestions that they could cause harmful, unintended impacts on human health as well as the environment. [8] Initially SF_6 was thought to be an improvement to oils used for the same purposes that contained harmful PCBs. Since it is a chemically inert gas, direct effects on human health are negligible. However, it can have detrimental effects on the environment which were unforeseen at the time of its rise in popularity.

Once released into the atmosphere, SF_6 is very long-lived with an atmospheric lifetime of approximately 3200 years. [5] This lifetime is a result of the nearly negligible oceanic uptake rates due to the low solubility of SF_6 in water and no known microbiological processes destroy the compound in plants or soils. The only known destruction process for SF_6 in our atmosphere takes place above 60km within the upper mesosphere and thermosphere by ultraviolet radiation at very short wavelengths less than 240nm. While the full extent of the SF_6 chemistry is not well understood, it is believed that the degradation process begins with an electron attachment forming SF_6^-. The electron attachment can be destructive, leading to the decay of the molecule, or it can leave SF_6^- in an excited state that undergoes further chemistry to ultimately yield HF. It is also believed that SF_6 does not react with OH radicals in the troposphere [9]

The longevity of SF_6 in the atmosphere combined with its effective absorption in radiatively important windows in the infrared region (radiative efficiency = 0.52 $W*m^{-2}*ppb^{-1}$) make SF_6 one of the most potent greenhouse gases. A global warming potential (GWP) compares other atmospheric gases to the greenhouse capabilities of CO_2. Upon comparison, the GWP of SF_6 over a 100 year timescale is 24000 times larger than that of CO_2. Despite this large effect on the warming of the atmosphere, SF_6 has contributed only 0.1% of the man-made global warming effect due to atmospheric concentrations that are approximately a factor of 10^8 lower than CO_2. [6] However, this contribution will continue to rise if actions are not taken to stop release of SF_6 into the atmosphere and mitigation of the current levels of SF_6 in the atmosphere since they cannot be eliminated naturally.

Nitrogen trifluoride (NF_3) is similar to SF_6 in that the industrial usage of the gas has grown rapidly over the past few decades. NF_3 first appeared in industry around the 1960s and 1970s in applications such as rocket fuel oxidizer and a fluorine atom donor for use in chemical lasers. [10] The use of NF_3 in mainly specialty applications helped to limit the emissions into the atmosphere. However, beginning in the 1990's more regular industrial usage of NF_3 began in the manufacture of semiconductors and both plasma and LCD flat panel display devices. In these applications, NF_3 is mainly used as a fluorine donor where it is broken down to form highly reactive F atoms and radicals. Once broken down, these F atoms and radicals then go on to react with and remove silicon containing contaminants in the process chambers of the electronics being manufactured. [10]

NF_3 follows the same storyline as SF_6 described above. Initially NF_3 was thought to be a safer alternative to the perfluorocarbons (PFCs), mainly hexafluoroethane, which had been used for the same purposes in electronics manufacturing. The fact that NF_3 was a much safer gas to transport due to its stability and nonflammable nature compared to the PFCs.[10,11] NF_3 was also preferable to PFCs due to faster cleaning rates and higher efficiency. It was believed that NF_3 was an environmentally safer alternative due to its supposed higher conversion efficiencies which would help industries meet their emission reduction requirements. Conversion efficiencies to form reactive F atoms and radicals were only ~30% for hexafluorethane and ~98% for NF_3. [10]

The higher efficiency of NF_3 compared to its PFC counterpart did reduce emissions of electronics manufacture. According to Arnold *et al.* "the emissions benefit of using NF_3 over hexafluoroethane (C_2F_6) in electronics manufacture is significant—emissions of between 53 and 220 Tg CO_2-eq·y^{-1} were avoided during 2011." Despite this, the detrimental effects that anthropogenic NF_3 released into the atmosphere could have on global climate has been overlooked. The radiative efficiency of NF_3 is 0.211 $W*m^{-2}*ppb^{-1}$, contributing to the fact that the global warming potential of NF_3 over a 100 year timespan is nearly 17,000 times higher than that of CO_2 [10]. The main atmospheric sink for NF_3 once it has been released into the atmosphere is photolysis in the stratosphere, but recently studies have suggested that reaction with $O(^1D)$ also plays a significant role in determining the fate of NF_3. [12] Nevertheless, the atmospheric lifetime of NF_3 is nearly five times longer than that of CO_2 making it a potent GHG.

Many believed that the high conversion rate of NF_3 limited the amount that could escape into the atmosphere from industrial emissions and it was not covered by the original 1997 Kyoto protocol as a result. As recently as 2006, the techniques available to measure NF_3 in the atmosphere were not sophisticated enough to make accurate measurement of a gas with as low a concentration of NF_3. It was estimated that in 2006 the global atmospheric burden of NF_3 was 1,200 metric tons, while recent measurements suggest that the actual amount was closer to 4,200 metric tons. In 2008 the measured amount of NF_3 in the atmosphere was approximately 5,400 metric tons, showing an annual increase of around 11%. [13] Due to this discovery, NF_3 was added to the list of gases in the Kyoto protocol in 2012. While the atmospheric burden of NF_3 is much smaller than that of CO_2 and many other GHGs, including SF_6, the fact that the emissions of such a potent GHG were so grossly underestimated is alarming.

INTRODUCTION
Part III: Water Complexes

Water is the most abundant GHG in the atmosphere, it is the direct cause of nearly 60% of the global warming trend.[14] Water vapor in the atmosphere provides the life-sustaining temperature that we experience. The addition of anthropogenic GHGs upsets the natural balance causing even more water vapor to evaporate into the atmosphere due to the increasing temperatures. As global temperatures continue to rise more water vapor will be present in the atmosphere where much of the atmospheric chemistry takes place. Due to its overwhelming abundance as well as its strong proclivity to form hydrogen bonds, water plays a key role in many atmospheric reactions. Some reactions involve water acting as a reactant in a bimolecular reaction but many other utilize a molecular complex with water molecules. It is believed that water molecules can stabilize other reactive species, such as ClO, OH, and HO_2, providing ample time for them to react.[15]

Whatever the reason is, there is no doubt that water molecules complex with other species in the atmosphere. The effect of the complexation on the absorption properties of the molecules involved compared to the monomers has been long neglected and underestimated. Consistent discrepancies between atmospheric measurements and theoretical model results incited many scientists to investigate the role that these molecular complexes play in the absorption of solar and terrestrial radiation.[16]

The spectral properties of molecular complexes are much different than those of the individual monomers. Complexation can lead to shifting and/or broadening of existing bands or generation of new absorption bands within the spectrum. On an individual scale the effect of this on the absorption capabilities of the molecules may seem small; for example Haedrick *et al.* state that "O_2-N_2 complexes contribute 2.2-3.11 W/m^2 to the total absorption from an overhead Sun during clear-sky conditions."[16] However when looking at the number of complexes that may be in the atmosphere at any given point in time, that amount of additional radiation absorption that this could generate is much more significant; especially since majority of the weak intermolecular interaction are typically IR active. [15,16]

Water complexes, as well as other molecular complexes, occurring in the atmosphere are a type of van der Waals complex. Van der Waals complexes are defined as "molecular systems in which the individual parts are held together by forces other than covalent bonds. These include ionic complexes (where the dominant attractive force is of electrostatic origin), complexes with hydrogen bonds, charge-transfer complexes, and true van der Waals molecules for which the dominant attractive contribution is the dispersion energy."[17] The strong hydrogen-bonding character makes it the preferred way for water to interact with other molecules, as it appeared in the case with water and NF_3.

However, recent studies suggest that there may be a more complex way through which NF_3 and H_2O interact. Dunitz and Taylor present studies to support that, in most cases, covalently bound fluorine hardly ever acts as a hydrogen bond acceptor compared

to anionic fluoride.[18] Dunitz and Taylor present theoretical calculations and come to the following conclusion; "It is interesting that in general fluorine atoms attached to carbon do not have significant power to act as proton acceptors in the formation of hydrogen bonds in the way that would be anticipated from the large difference in electronegativity of fluorine and carbon.[18]"

Although the molecules being investigated here involve fluorine covalently bound to sulfur, not carbon, it would seem that similar effects would probably occur. In fact, this phenomena is wide spread Weinhold and Klein actually assert that there should be a change in the way hydrogen bonds are defined: "Both direct and statistical lines of evidence point to the essential resonance covalency of H-bonding interactions, rather than the statistically insignificant ''dipole–dipole'' character that is persistently advocated in current textbooks.[19]" Considering the facts presented above, the interactions involved in the complexation of SF_6/NF_3 with water may be more complex than once previously believed.

MATRIX ISOLATION SPECTROSCOPY

The formation of the molecular complex H_2O-NF_3 has been previously investigated through the use of matrix isolation spectroscopy. The data presented below for the H_2O-NF_3 complex is courtesy of Jolayana Wold and Jonathan Boron. Matrix isolation spectroscopy is a method by which guest, analyte, molecules or atoms are trapped within a solid matrix. The matrix itself may be comprised of reactive or inert gases depending on the analysis being conducted but in order to solidify the matrix extremely low temperatures must be utilized. Most commonly matrices are comprised of an inert gas that is utilized to trap a species of interest by acting as a cage to prevent diffusion and most rotation. Ideally this can be utilized to trap transient or reactive species that would otherwise be difficult to detect.[20]

A diagram of the apparatus used in matrix isolation experiments is shown in Figure 3 below. Specifics of the matrix isolation cold cell can be found in Figure 3a while the set-up relative to the IR detector can be seen in Figure 3b. The gas mixture is deposited on a cold window which can be made of various materials including CsBr and CsI, both of which are fairly expensive. Therefore many people have turned to KBr windows for their matrix isolation experiments, including those presented here. Radiation shields are necessary to minimize exposure of the cold end of the refrigerator to external sources of blackbody radiation. The vacuum shields allow matrix isolation work to take

place below 10K. The deposition window is rotated within the cold cell in order to align he window with gas inlet for deposition or the IR beam to allow for scanning of the sample.

a)

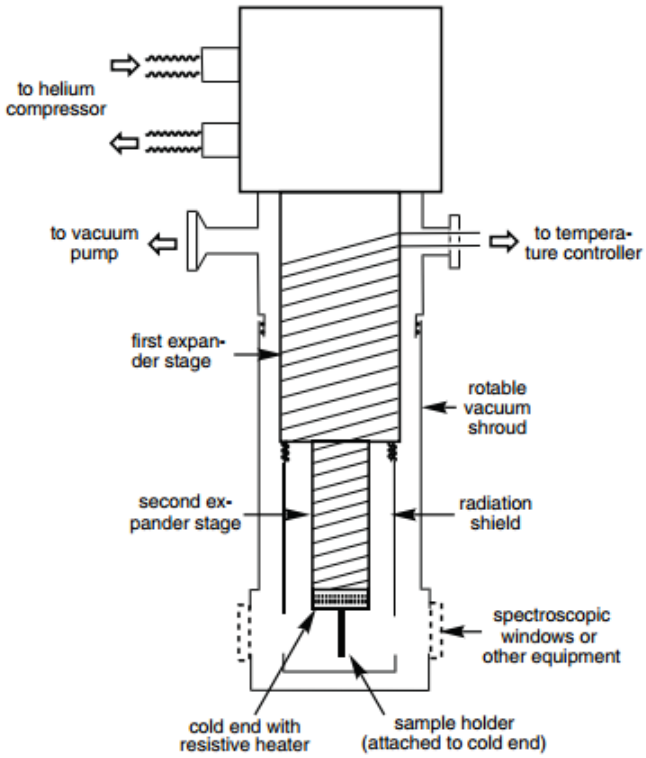

b)

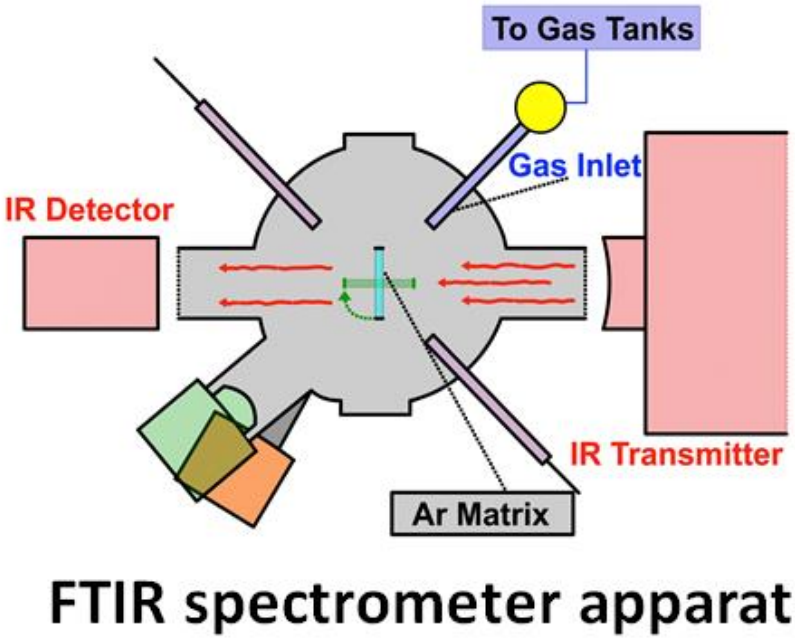

Figure 3: Schematic of matrix isolation instrumentation[20]

Once the sample is solidified into the matrix, various spectroscopic techniques can be employed such as Raman, UV-Vis absorption and IR spectroscopy. The H_2O-NF_3 complex was analyzed by depositing a matrix of H_2O, NF_3 and Ar onto a KBr window at 6K and an IR spectrum was collected. Differing ratios of water and NF_3 gas were mixed together with argon to a final pressure of 700 torr following by deposition of 200 torr of the mixture. Using an FTIR spectrometer with a resolution of 0.5 cm^{-1}, spectra of the various mixtures were collected in the mid-infrared region from 500cm^{-1} to 4500cm^{-1}.

H_2O-NF_3 EXPERIMENTAL STUDIES
Part I: Theoretical Calculations

Computational studies of this van der Waals complex were also carried out utilizing the CCSD level of theory (coupled cluster with singles and doubles). CCSD is a post-Hartree-Fock *ab initio* method which improves on the Hartree-Fock molecular orbital method by utilizing multi-electron wavefunctions to account for electron correlation.[21] The optimized geometry features hydrogen bonding of both hydrogen atoms on the water molecules coordinated with two of the three fluorine atoms of the NF_3. The optimized geometry and the vibrational frequencies for the complex can be seen in Figure 2 and Table 1 respectively.

a)

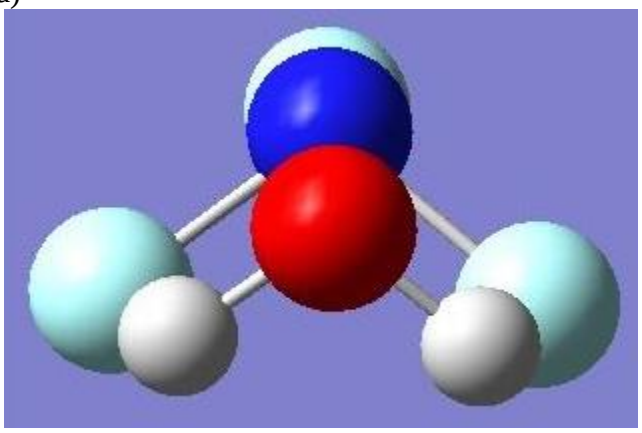

b)

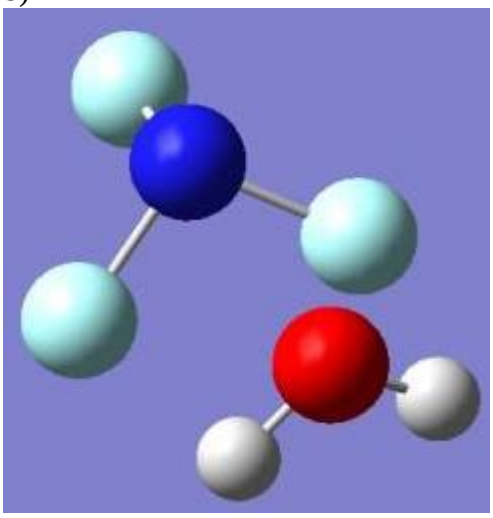

Figure 4: Optimized geometry for the H_2O-NF_3 complex[22]

Table 2: Density functional theory: CCSD (Basis Set: cc-pVTZ) calculation results for H_2O-NF_3 van der Waals complex [22]

H_2O-NF_3	NF_3	H_2O	$\Delta\nu$ (cm^{-1})
524.0[a] (0.1099)[b]	522.9 (0.03460)	-	1.1
685.8 (3.339)	686.0 (3.283)	-	0.2
1006 (189.4)	1015 (199.7)	-	9
1011 (202.6)	1015 (199.6)	-	4
1094 (38.43)	1100 (38.35)	-	6
1680 (61.74)	-	1678 (66.08)	2
3875 (4.962)	-	3876 (4.483)	1
3977 (42.60)	-	3979 (43.31)	2

[a] Frequencies (cm^{-1})
[b] Band intensity

H_2O-NF_3 EXPERIMENTAL STUDIES
Part II: Matrix Isolation Experiments

The results of the IR analysis revealed two peaks, one at 1591cm^{-1} and the other at 3730cm^{-1} that were identified as the complex. As shown in the table of vibrations above, complexation with NF_3 causes a shift in the vibrational frequencies of the non-rotating monomer (nrm). Once the nrm peak is identified in a spectrum it indicates clear locations in which to look for the shifted peak resulting from the complex. An example IR spectrum from this experiment is show below.

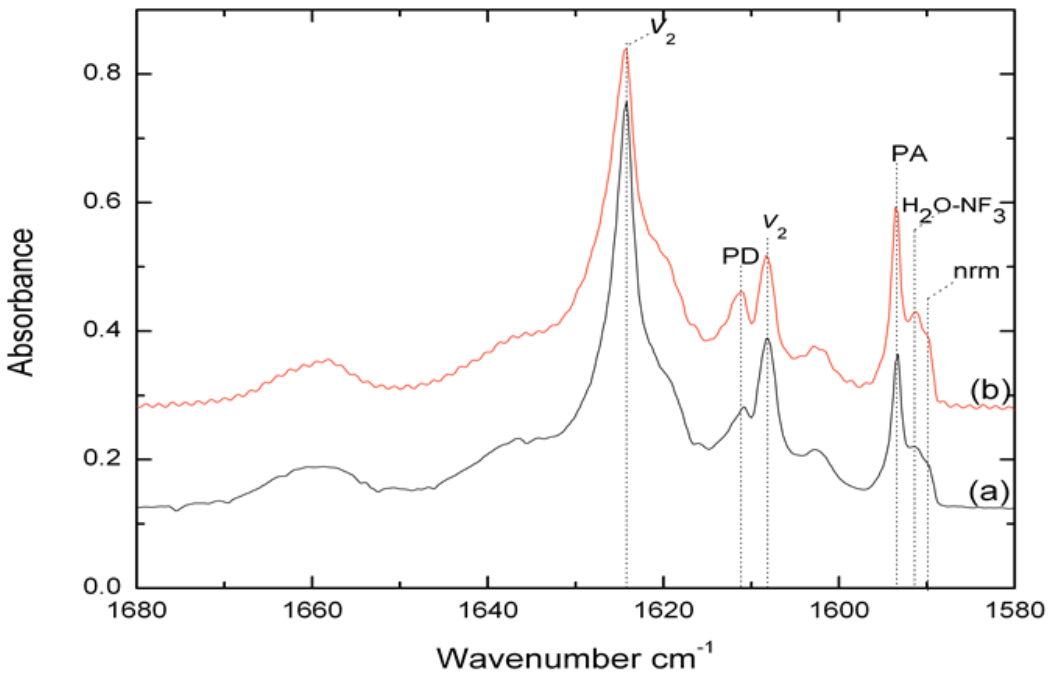

(a) 1:100 H_2O:Ar (b) 0.1:1:100 NF_3:H_2O:Ar

Figure 5: Peak identification of H_2O-NF_3 complex in the 1680-1580 cm^{-1} region[22]

The assignment of this peak was further confirmed by concentration studies. The concentration of H2O was held constant as the concentration of NF3 was increased. If the peak was correctly identified as belonging to the H2O-NF3 complex, then the peak height should increase as the concentration of complex is increased by increasing the NF3 concentration. Increasing the NF3 concentration caused a direct increase in the observed peak height of the peak at 1591cm-1.

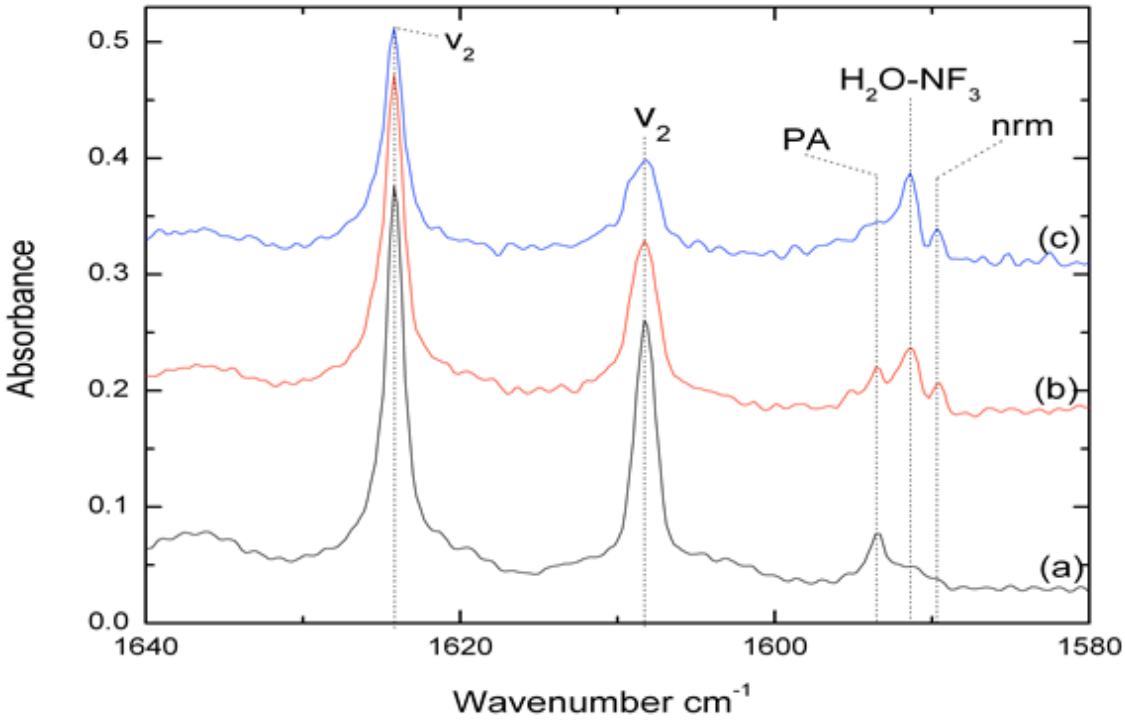

(a) 2:1000 H_2O:Ar
(b) 2:5:1000 H_2O:NF_3:Ar
(c) 2:10:1000 H_2O:NF_3:Ar
Figure 6: Concentration studies of water and NF_3 in an argon matrix[22]

From the experiments completed so far, it is evident that fluorine containing compounds in the atmosphere do form van der Waals complexes with water. It was not clear however, on the exact nature of the interaction between NF_3 and water. It appears as though there is a hydrogen bonding interaction taking place based on the optimized structure. It is also possible that there is no actual H-bonding taking place and water is simply orienting itself along the dipole generated by the NF_3 molecule. Nevertheless, in order to further examine the effect that water complexes have on the IR spectra of fluorine containing compounds, SF_6 water complexes were analyzed with similar methods.

H_2O-SF_6 EXPERIMENTAL STUDIES
Part I: Theoretical Calculations

The optimized geometries for the H_2O-SF_6 complexes were calculated using the GAUSSIAN[23] program using the B3LYP and WB97XD levels of theory with various basis sets ranging from 6-31G (2d, 2P) to CC-pVTZ. B3LYP is a hybrid functional theory which includes a mixture of Hartree-Fock exchange with DFT exchange-correlation. The non-local correlation is provided by the correlation functional of Lee, Yang, and Parr (LYP), while the local correlation is provided by the Vosko, Wilk, and Nusair 1980 correlation (VWN) functional III.[24,25] While B3LYP works well for most systems, at large distances, as is present in a van der Waals complex, it can become inaccurate. This is due to the non-Coulomb part of the exchange functional dying off too rapidly making it highly inaccurate at large distances.[26]

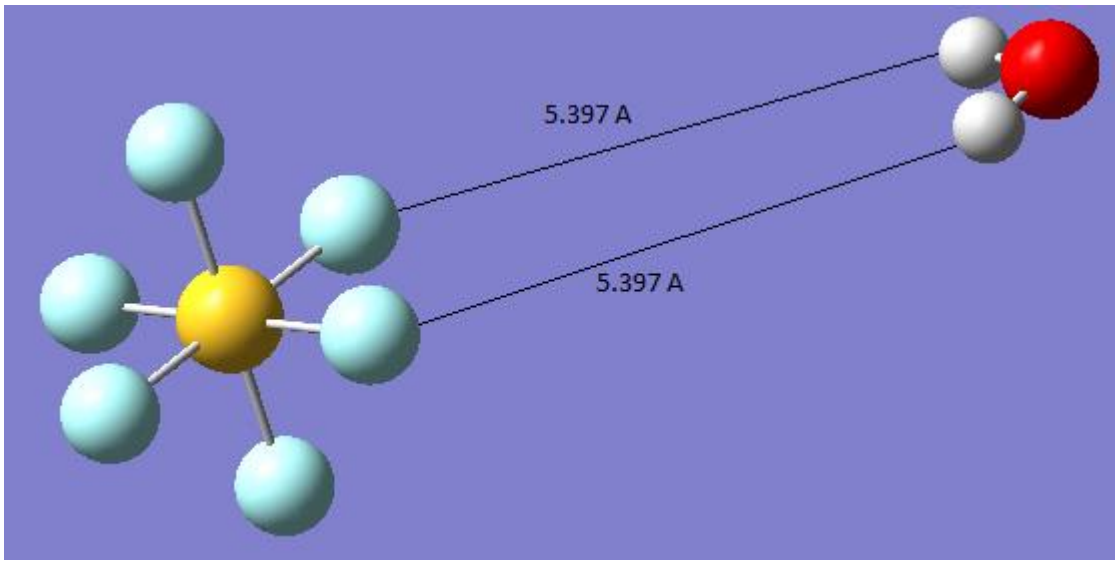

Figure 7:H_2O-SF_6 optimized geometry- DFT with B3LYP calculation method and aug-CC-pVTZ basis set

The far intermolecular distance coupled with the existence of several imaginary frequencies, indicated that the B3LYP level of theory did not work well for this type of complex. After consulting Dr. Henrik Kjaergaard from the University of Copenhagen it was decided that the WB97XD functional theory would be more applicable for the long-range interaction present in the H_2O-SF_6 complex.

Head-Gordon and Chai developed the WB97XD functional that includes empirical atom-atom dispersion corrections as well as long-range corrections making it much more suitable for the type of interactions in the H_2O-SF_6 van der Waals complex.[26] Utilizing this functional theory the basis sets were varied beginning at 6-31G (2d, 2P) ending with the highest level basis set utilized in this experiment, cc-pVTZ. Figure 6 depicts the preliminary calculations which utilized the WB97XD functional, while Figure

7 illustrates the final optimized geometry (additional summaries for lower level calculations can be found in the Appendix).

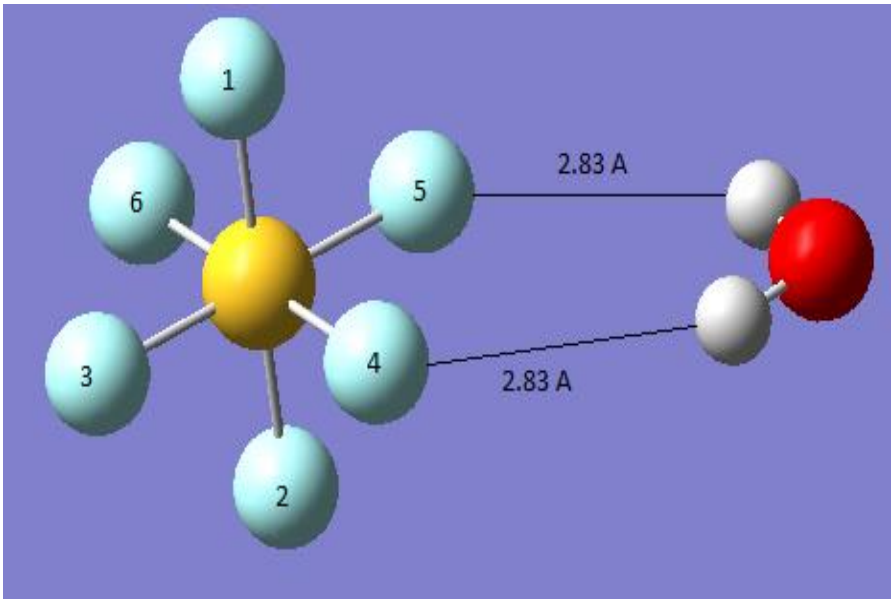

Figure 8: H_2O-SF_6 optimized geometry- DFT with WB97XD calculation method and 631G++ basis set

Table 3: Bond angle differences (DFT with WB97XD calculation method and 631G++ basis set)

SF_6			
Angle Between Atoms	**Monomer**	**Dimer**	**Difference**
1-2	180.00	179.55	-0.45
1-3	90.00	90.16	0.16
1-4	90.00	89.84	-0.16
1-5	90.00	89.84	-0.16
1-6	90.00	90.16	0.16
2-3	90.00	90.16	0.16
2-4	90.00	89.84	-0.16
2-5	90.00	89.84	-0.16
2-6	90.00	90.16	0.16

3-4	90.00	89.98	-0.02
4-5	90.00	89.74	-0.26
5-6	90.00	89.98	-0.02
3-6	90.00	90.29	0.29
3-5	180.00	179.72	-0.28
4-6	180.00	179.72	-0.28
Water			
	104.10	104.84	0.74

Table 4: Vibrational frequencies of the complex compared to individual monomers calculated using ultrafine convergence criteria and 631G++ basis set (DFT-WB97XD)

H_2O-SF_6	**H_2O**	**SF_6**	**$\Delta\nu$ (cm^{-1})**
-63.76 (88.07)	-	-	-
-19.33 (0.79)	-	-	-
30.10 (6.86)	-	-	-
37.50 (0.00)	-	-	-
40.26 (0.11)	-	-	-
110.81 (209.94)	-	-	-
317.31 (0.02)	-	316.71 (0.00)	0.60
317.38 (0.01)	-	316.71 (0.00)	0.67
317.86 (0.00)	-	316.71 (0.00)	1.15
490.82 (0.03)	-	489.40 (0.00)	0.79
491.19 (0.00)	-	489.40 (0.00)	1.79
491.28 (0.01)	-	489.40 (0.00)	1.88
574.98 (27.00)	-	568.52 (53.55)	6.46

575.80 (26.48)		568.52 (53.55)	7.28
576.26 (22.72)	-	568.52 (53.55)	7.74
624.08 (0.19)	-	615.57 (0.00)	8.51
625.46 (0.48)	-	615.57 (0.00)	9.89
728.42 (0.51)	-	726.34 (0.00)	2.08
915.83 (386.46)	-	870.04 (570.18)	45.79
915.85 (443.51)	-	870.04 (570.18)	45.81
916.79 (405.26)		870.04 (570.18)	46.75
1642.13 (114.93)	1636.08 (82.20)	-	6.05
3907.91 (12.13)	3905.03 (9.27)	-	2.88
4019.50 (53.05)	4019.27 (4019.27)		0.23

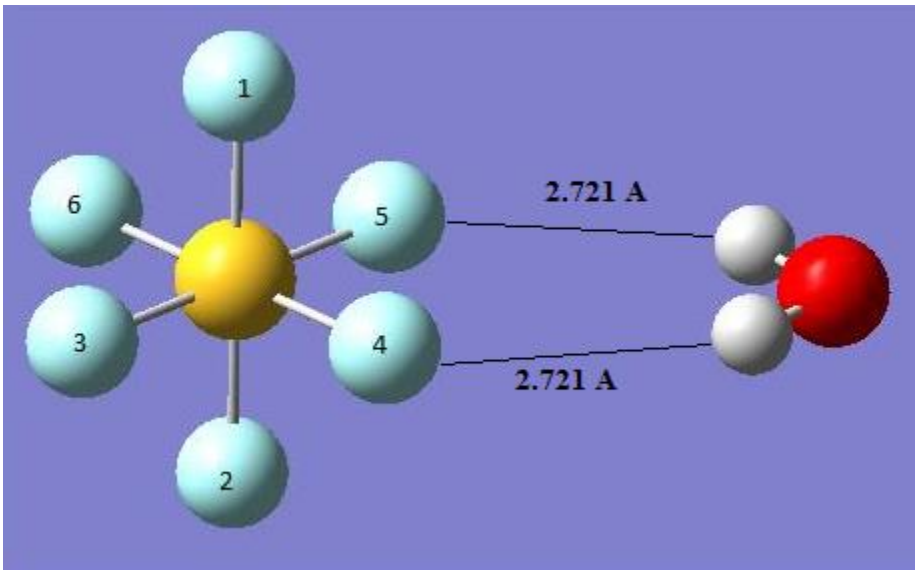

Figure 9: H_2O-SF_6 optimized geometry- DFT with WB97XD calculation method and CC-pVTZ basis set

Table 5: Bond Angle Differences (DFT with WB97XD calculation method and CC-pVTZ basis set)

SF_6			
Angle between atoms	**Monomer**	**Dimer**	**Difference**
1-2	180.00	179.75	0.25
1-3	90.00	90.09	0.09
1-4	90.00	89.91	0.09
1-5	90.00	89.91	0.09
1-6	90.00	90.09	0.09
2-3	90.00	90.09	0.09
2-4	90.00	89.91	0.09
2-5	90.00	89.91	0.09
2-6	90.00	90.09	0.09
3-4	90.00	89.96	0.04
4-5	90.00	89.91	0.09
5-6	90.00	89.96	0.04
3-6	90.00	90.16	0.16
3-5	180.00	179.87	0.13
4-6	180.00	179.87	0.13
Water			
	104.10	104.25	0.15

As can be seen in the table above, there are notable differences between the bond angles of both H_2O and SF_6. Some of the IR vibrations of SF_6 are normally invisible in the IR due to the symmetry of the molecule. Once complexed with water the symmetry of the SF_6 molecule is altered, making those once invisible vibrations visible to the IR. The vibrations of the optimized structure, as predicted by Gaussian are shown in Table 3 below.

Table 6: Vibrational frequencies of the complex compared to individual monomers calculated using ultrafine convergence criteria and cc-pVTZ basis set (DFT-WB97XD)

H_2O-SF_6	H_2O	SF_6	$\Delta\nu$ (cm^{-1})
-86.42[a] (71.84)[b]	-	-	-
-31.56 (117.5)	-	-	-
58.18 (0.3021)	-	-	-
64.27 (194.7)	-	-	-
88.76 (57.20)	-	-	-
93.24 (0.00)	-	-	-
338.3 (0.00)	-	339.9 (0.00)	-1.6
339.2 (0.0287)	-	339.9 (0.00)	-0.7
339.4 (0.1815)	-	339.9 (0.00)	-0.5
509.4 (0.00)	-	510.0 (0.00)	-0.58
509.4 (0.0155)	-	510.0 (0.00)	-0.58
509.7 (0.0348)	-	510.0 (0.00)	-0.28
595.4 (57.03)	-	596.2 (54.28)	-0.75
596.1 (54.17)		596.2 (54.28)	-0.05
597.2 (49.06)	-	596.2 (54.28)	-0.05
630.3 (0.1499)	-	634.4 (0.00)	-4.1
634.5 (0.3374)	-	634.4 (0.00)	0.12
768.3 (0.6341)	-	769.7 (0.00)	-1.4

904.9 (569.8)	-	910.8 (582.3)	-5.9
905.7 (610.7)	-	910.8 (582.3)	-5.1
911.9 (580.1)		910.8 (582.3)	1.1
1639.6 (119.7)	1639.7 (97.96)	-	-0.10
3880.9 (21.04)	3872.0 (15.40)	-	8.9
3974.2 (76.76)	3962.9 (80.12)		11.3

[a] Frequencies (cm^{-1})
[b] Band intensity

It should be noted that some imaginary frequencies still remain in the optimized structure. Imaginary frequencies are indicative of vibrations that would breakdown the structure, however imaginary frequencies of approximately 100 or less can generally be ignored for the purposes being explored here. From Table 3 above it can be ascertained that notable frequency shifts occur which could be helpful in identifying the complex. First, the SF_6 blue shift of approximately $6cm^{-1}$ around 910 cm^{-1}, as well as the larger magnitude blue shifts associated with the vibrations of the water molecule, are large enough that they should be identifiable in the experimental spectrum. It is also of importance to note that the potential energy surface of this interaction is extremely shallow, emphasizing weak nature of the underlying interactions. Unlike NF_3, SF_6 does not have a permanent dipole moment. Therefore it is possible that the SF_6 interaction is even weaker than that of NF_3, if in fact the nature of the interaction is not due solely to hydrogen bonding, making the complex even more difficult to detect.

H_2O-SF_6 EXPERIMENTAL STUDIES
Part II: Matrix Isolation Experiments

Initially, the concentrations of both SF_6 and water had to be optimized in order determine the ideal concentration at which to mix the two gases. The spectra of the individual components were gathered by depositing either SF_6 or H_2O in an inert argon matrix onto a cold window comprised of KBr at 6K. Then the resulting matrix was scanned using an FTIR spectrometer. Figures 10 and 12 show the effect of concentration on the spectra of SF_6 and H_2O respectively.

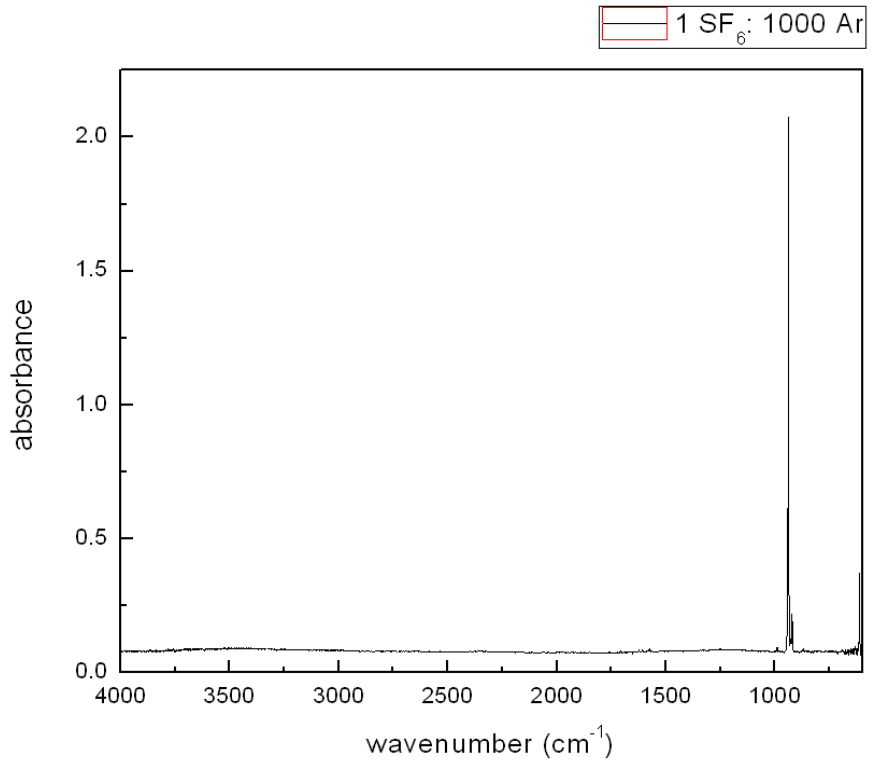

a)

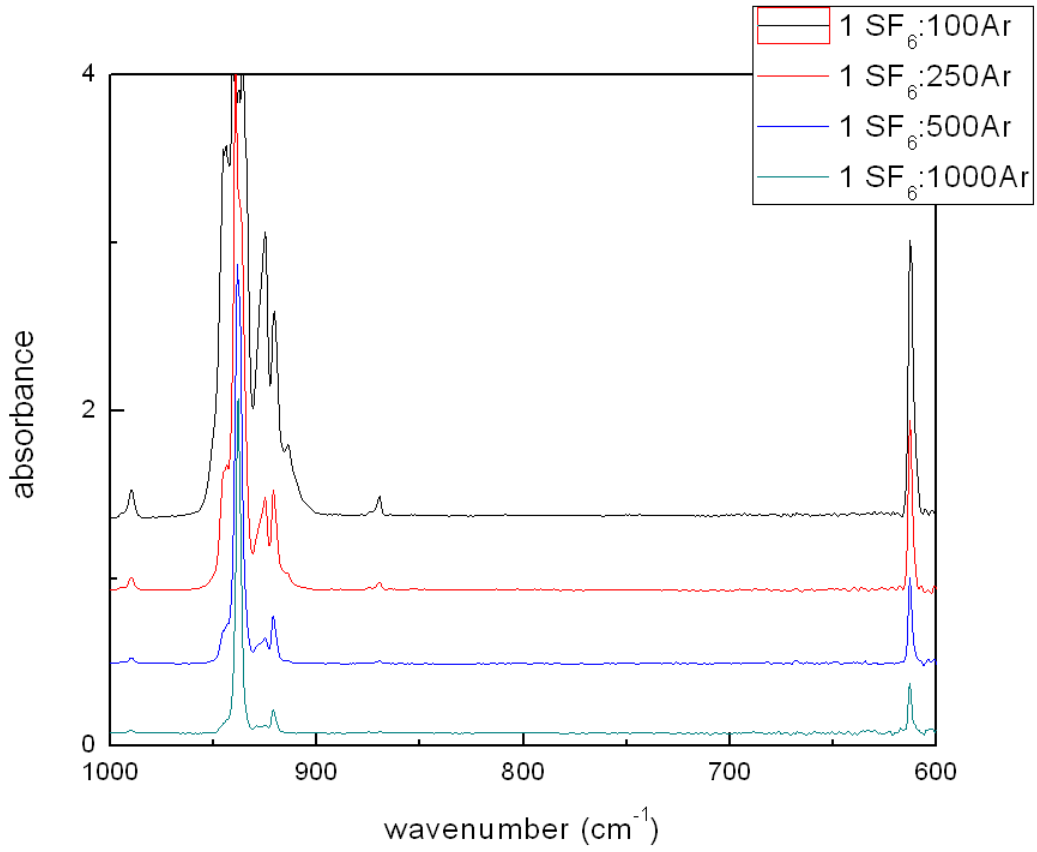

b)

Figure 10: a) Complete spectrum of SF_6 b)Magnified IR spectrum at various concentrations

The SF_6 spectrum does not have many differing features. It absorbs very strongly at 938cm^{-1} with minimal other characteristic peaks in the spectrum. In fact, there are only 2 IR active peaks associated with SF_6, ν_3 and ν_4. The other smaller peaks are a result of a mixture of one of these two IR active modes with a non-IR active mode.

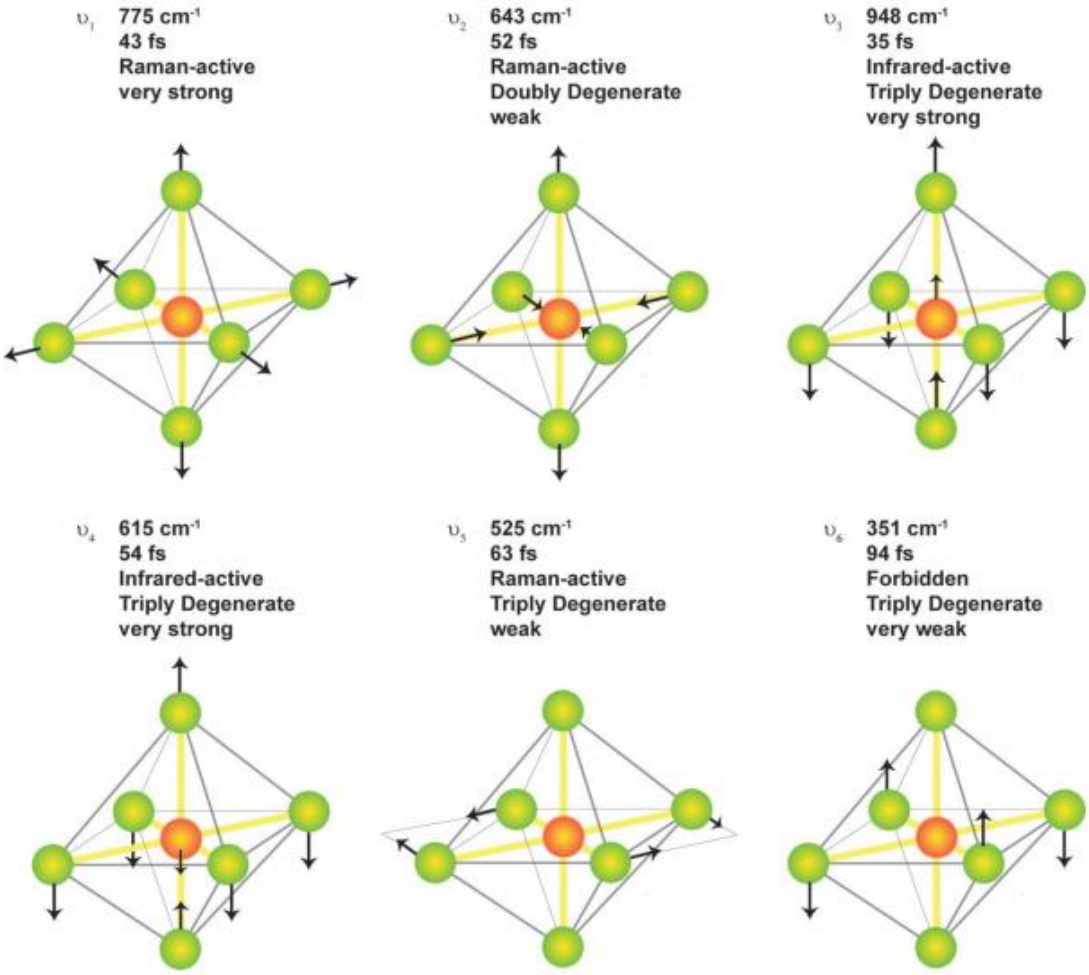

Figure 11: Vibrational modes of SF_6[27]

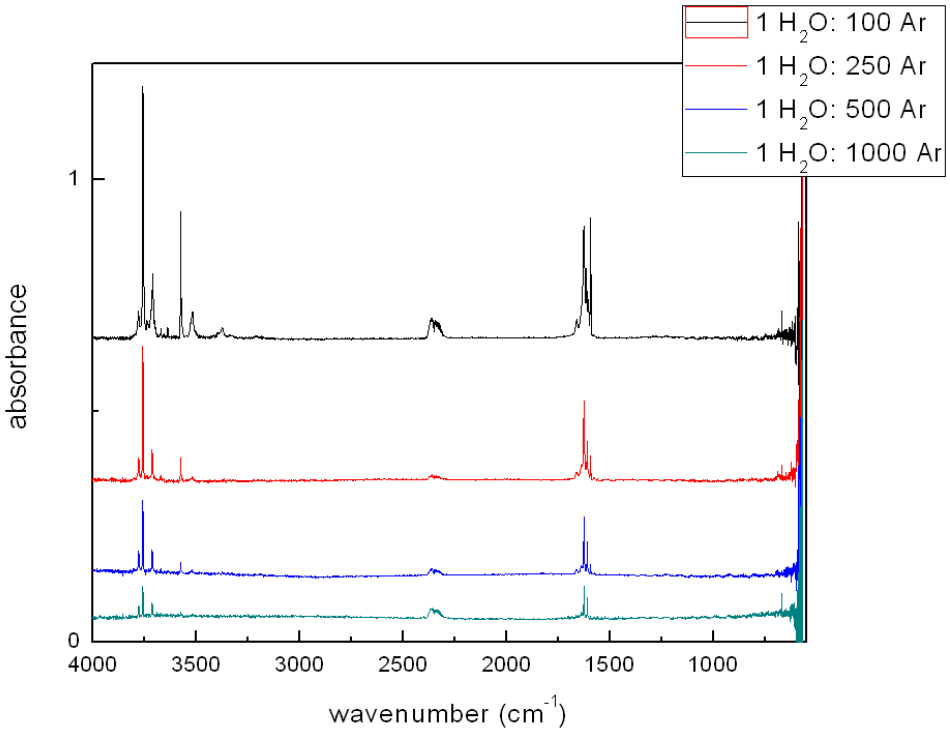
1 H2O: 100 Ar
1 H2O: 250 Ar
1 H2O: 500 Ar
1 H2O: 1000 Ar
absorbance
1
0
4000
3500
3000
2500
2000
1500
1000
wavenumber (cm-1)

a)

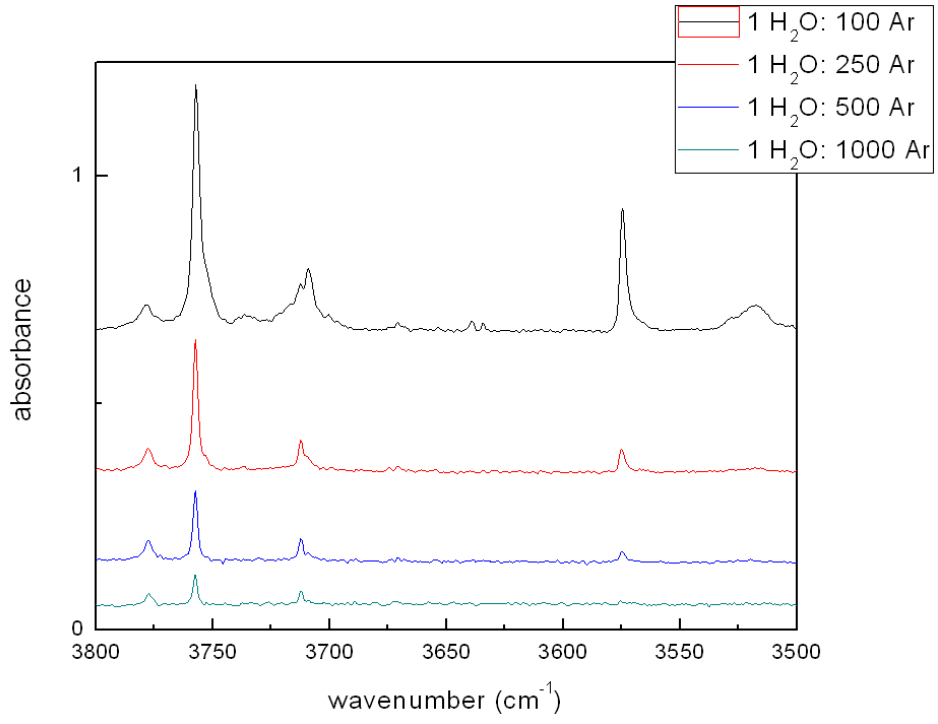
1 H2O: 100 Ar
1 H2O: 250 Ar
1 H2O: 500 Ar
1 H2O: 1000 Ar
absorbance
1
0
3800
3750
3700
3650
3600
3550
3500
wavenumber (cm-1)

b)

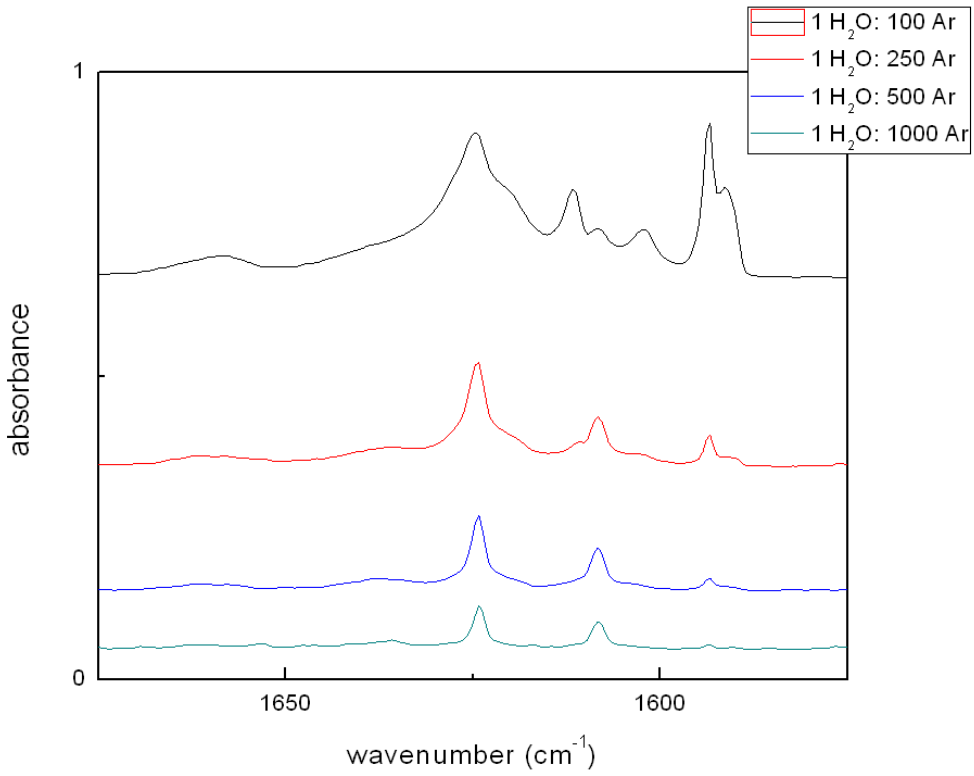

c)

Figure 12: a) H_2O IR spectrum at various concentrations
b) and c) magnified IR spectra of absorbing regions

From the IR spectrum of water, the key peaks of interest are those of the non-rotating monomer (nrm). Shifts calculated theoretically correspond to shifts of the nrm peaks in the spectrum. Other peaks are either rovibrational in nature or are the result of dimers, trimers, or multimers that occur as a result of aggregation of molecules within the matrix. The grouping of peaks from approximately 1575cm^{-1} to 1675cm^{-1} are the result of the ν_2, or bending mode, associated with the water molecule. In this region the nrm peak can be identified around 1590cm^{-1} and it is from this peak that shifts would be assigned based on the GAUSSIAN calculations.[28] However, the theoretical calculations showed

little, to no shift in this region (-0.10cm^{-1} as shown in Table 5). Therefore, unlike the NF_3-H_2O complex, the complexation with SF_6 shows no appreciable shift in this particular water nrm peak.

Another nrm peak exists in the ν_1 and ν_2 stretching regions of the spectrum which includes the range of 3500cm^{-1} to approximately 3800cm^{-1}. The nrm peak in this region occurs at about 3736cm^{-1}.[28] Table 5 shows that there is a sizable shift associated with the nrm in this region upon complexation with SF_6. This was one of the key peaks used to identify the H_2O-NF_3 complex in previous studies making this an ideal place to begin the investigation. However, this nrm peak is very weak and shows up very small in the IR spectrum (Figure 12) making it more difficult to distinguish a shifted peak due to the complex that would be even smaller in magnitude.

The spectra of 1 SF_6:100 Ar and 1 H_2O:100 Ar were each compared to the spectrum of the mixture 1SF_6:1H_2O:100Ar.

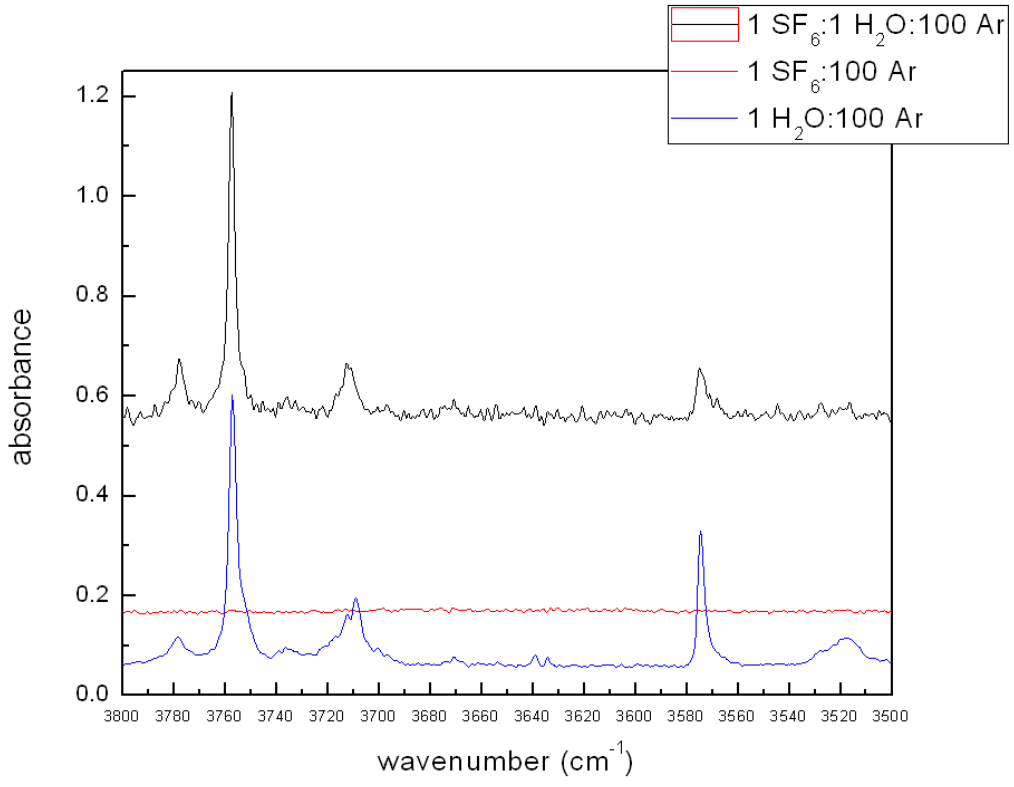
1 SF6:1 H2O:100 Ar
1 SF6:100 Ar
1 H2O:100 Ar
absorbance
1.2
1.0
0.8
0.6
0.4
0.2
0.0
3800 3780 3760 3740 3720 3700 3680 3660 3640 3620 3600 3580 3560 3540 3520 3500
wavenumber (cm-1)

a)

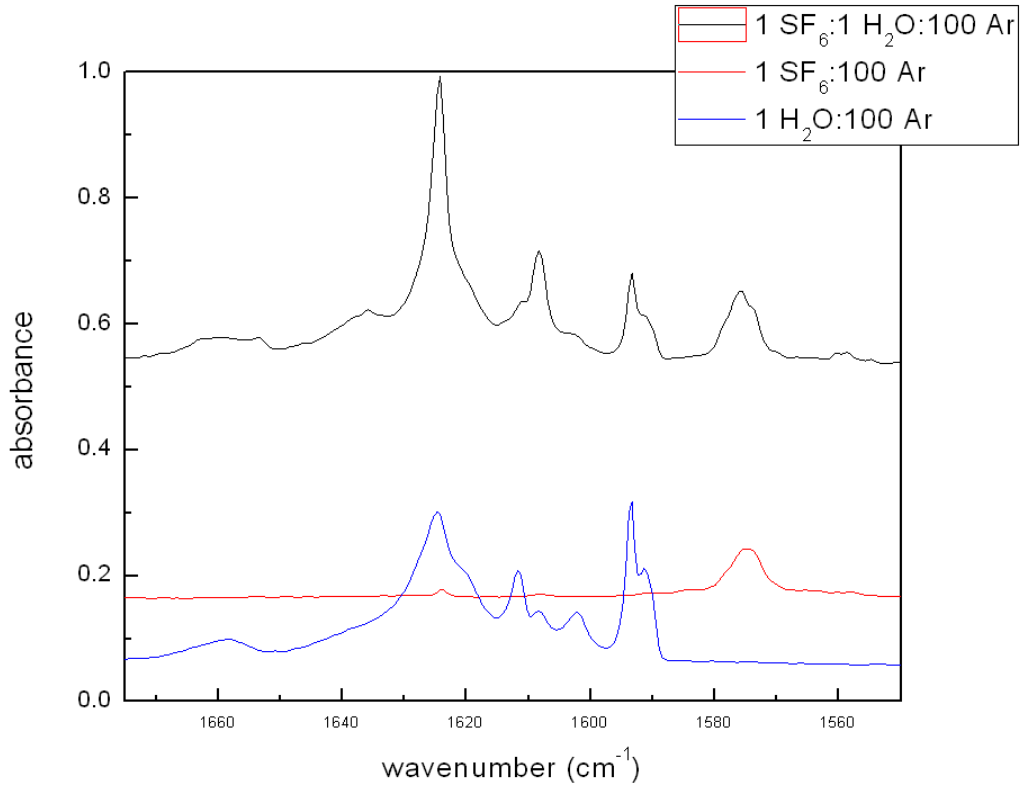
1 SF6:1 H2O:100 Ar
1 SF6:100 Ar
1 H2O:100 Ar
absorbance
1.0
0.8
0.6
0.4
0.2
0.0
1660 1640 1620 1600 1580 1560
wavenumber (cm-1)

b)

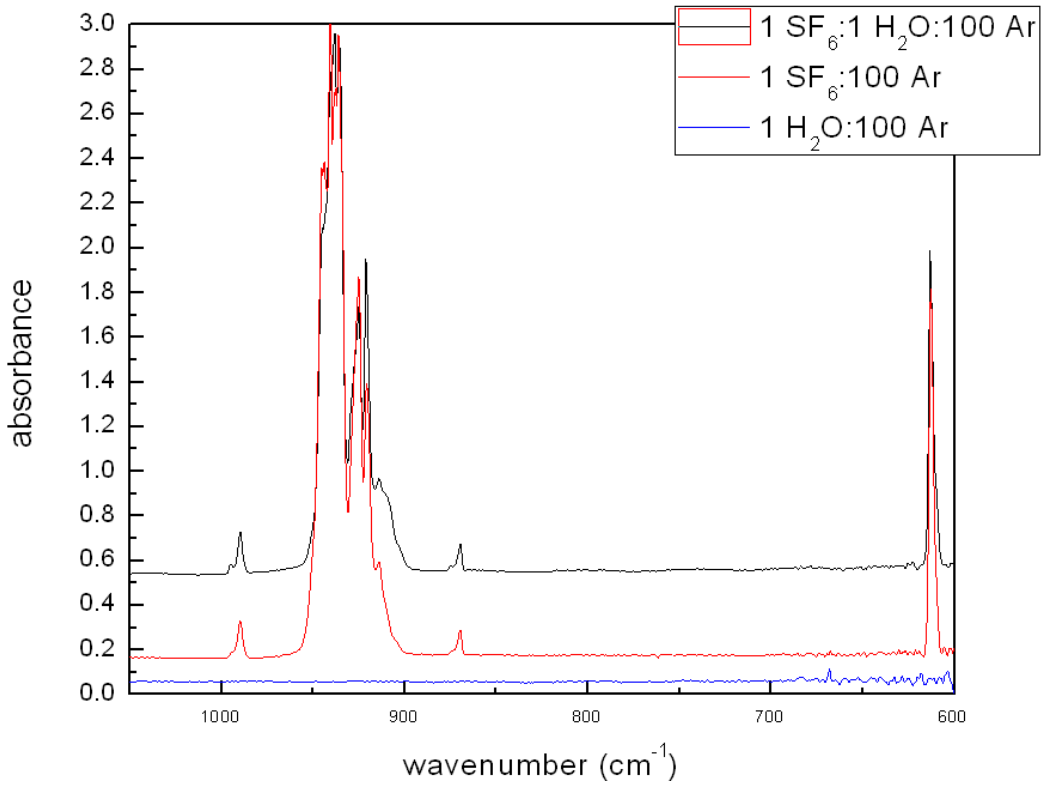

c)

Figure 13: Comparison of 1 H_2O:100Ar and 1 SF_6: 100Ar spectra to that of 1 SF_6:1 H_2O:100Ar mixture

From this comparison, no obvious distinction can be made regarding peak assignments for the H_2O-SF_6 complex. However, the lack of an obvious peak is not unexpected since the interaction itself is so weak and the amount of complex present is minute.

In order to further evaluate the presence of a peak due to the complex, concentration studies were carried out by altering the concentration of SF_6. Changing the concentration of one of the components may decrease the concentration of the complex but it will also decrease the absorbance of the sizable SF_6 peaks, possibly allowing originally obscured peaks to be revealed. Additionally, if the peak due to the complex

could be identified, the size of said peak would increase as the concentration of SF_6 increased thereby solidifying the assignment.

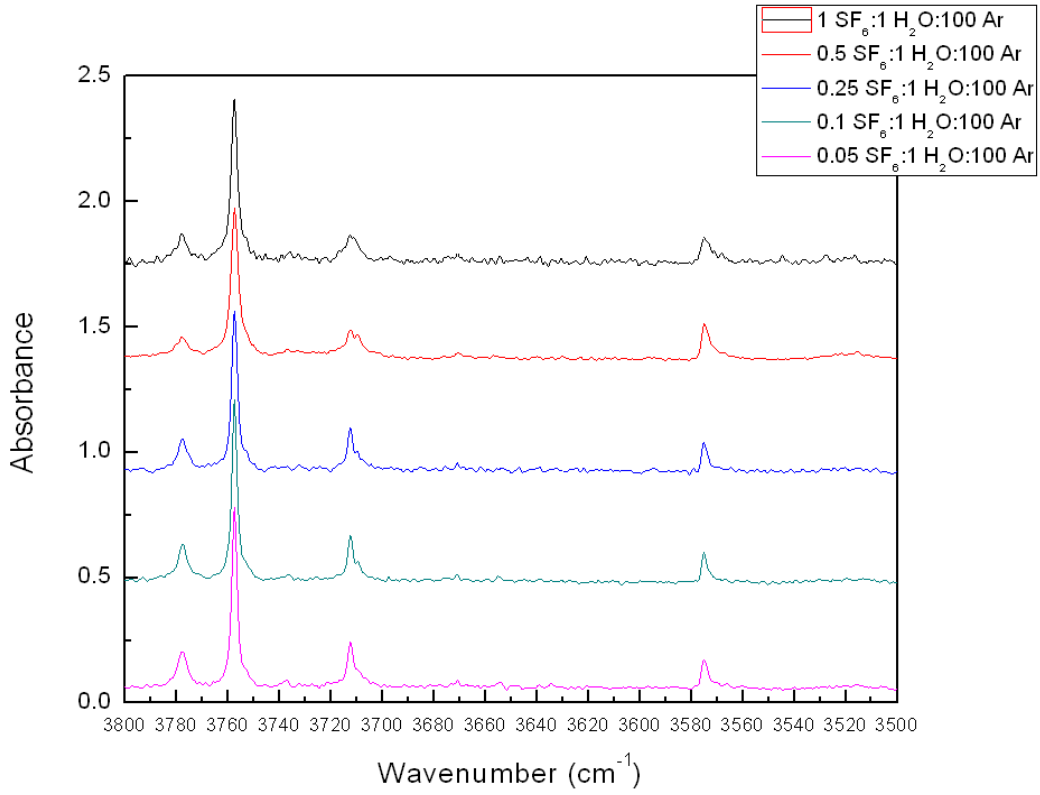

a)

b)

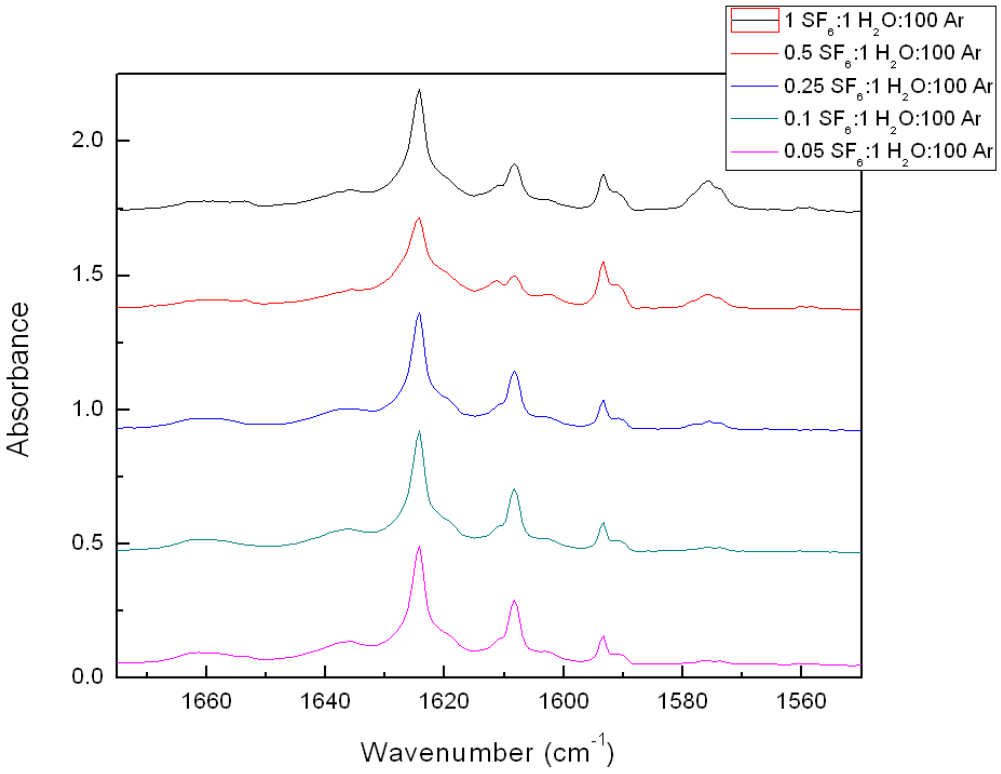

c)

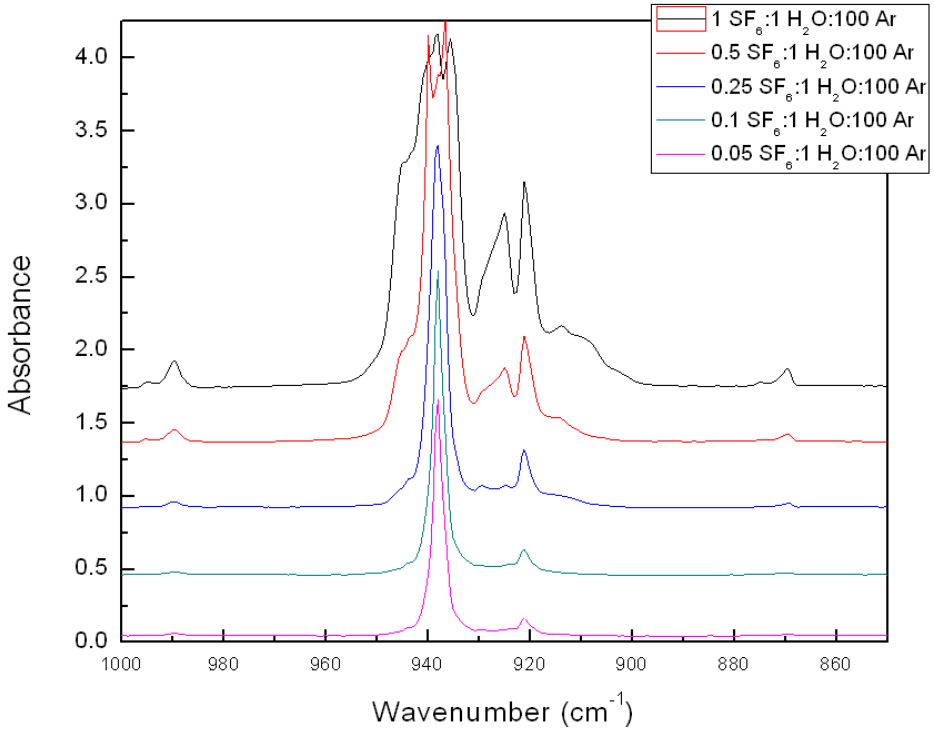

Figure 14: Concentration Studies - Increasing SF_6 concentration

As can be seen in the above figures, there was little appreciable difference between the trials within the H_2O stretching region and the only differences in the range of 900-1000cm^{-1} could be assigned to increasing SF_6 concentration alone. However, the strong absorbing properties of SF_6 in this region make small peaks that would be associated with the complex difficult to detect. Therefore, in order to better evaluate the possibility of peak shifts as a result of complexation, the SF_6 was held at low concentration while the H_2O concentration was increased. If a suspect peak could be identified, the intensity of such a peak would increase as the complex concentration is increased due to the increasing water concentration.

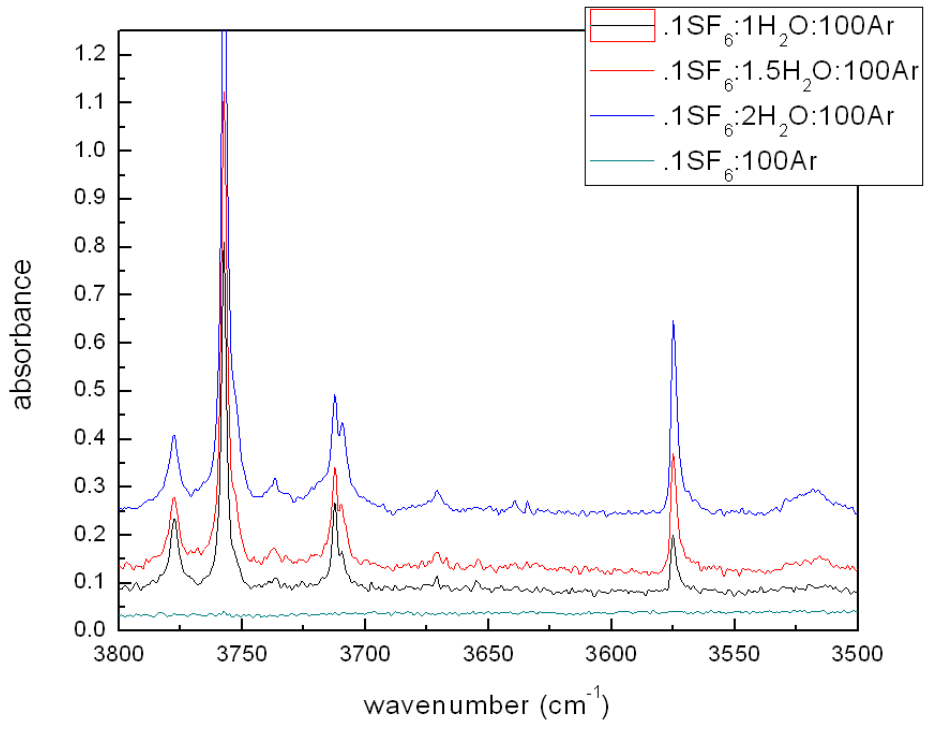

a)

b)

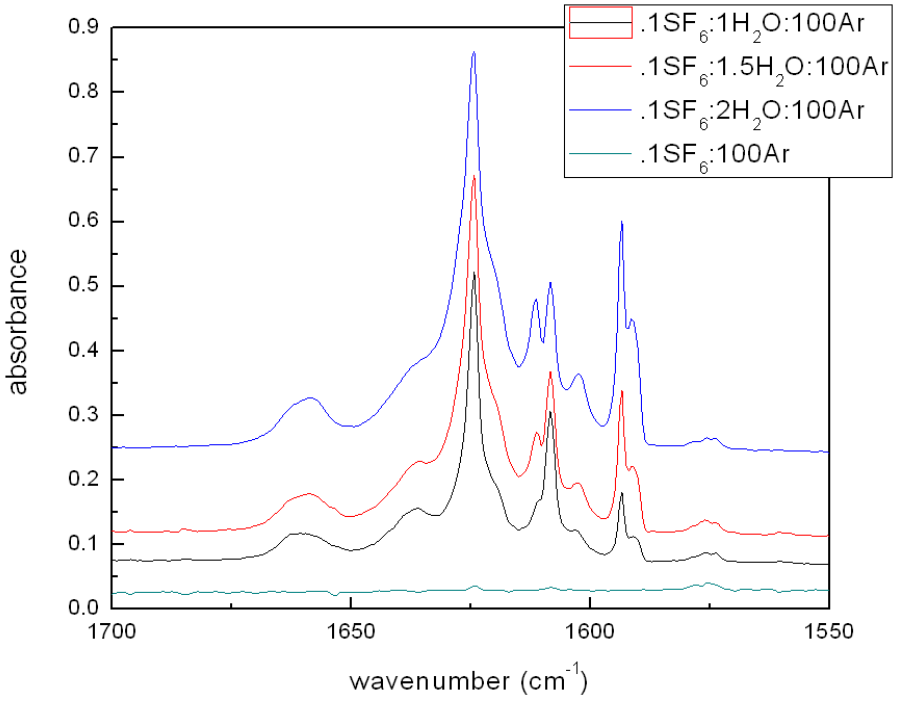

c)

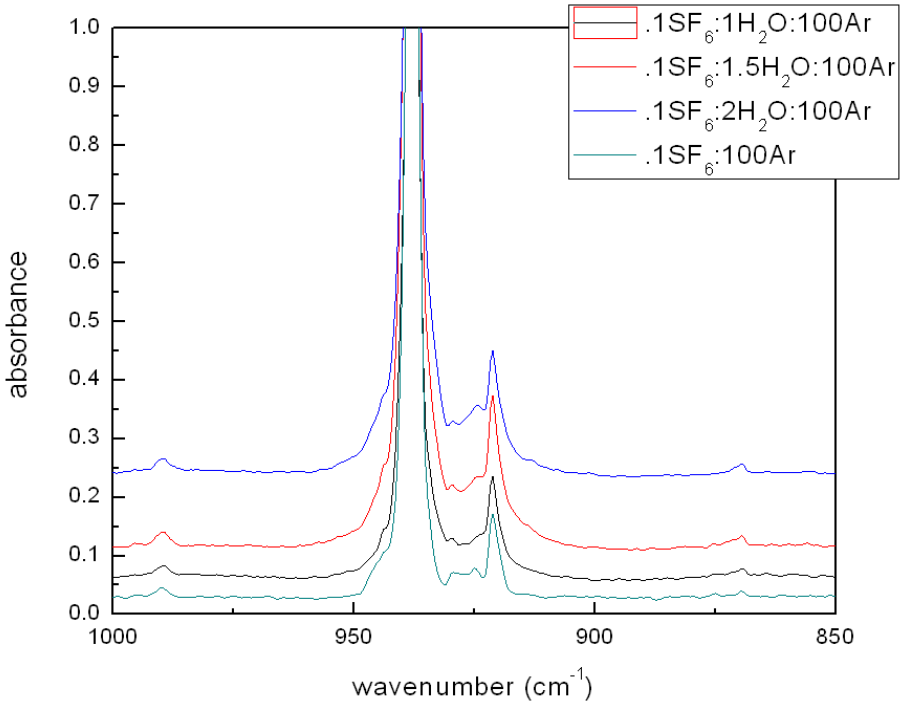

Figure 15: Concentration Studies – Increasing H_2O Concentration

The concentration studies of increasing water concentration did not reveal much novel information either. The H_2O bending regions did not expose any further candidate peaks for the shift of the nrm band at 3736cm-^{1}. Similarly, the absorbing region of SF_6 did not divulge further information regarding the shift of the SF_6 peak centered around 938cm^{-1} mainly due to the strength of the SF_6 peaks in this region. Even at this lower SF_6 concentration, the relative absorbance values of the strongest SF_6 peak was still too large to make any plausible classifications of band shapes. Therefore, in order to more fully evaluate this area of the spectrum, further trials had to be conducted at even lower concentrations of SF_6.

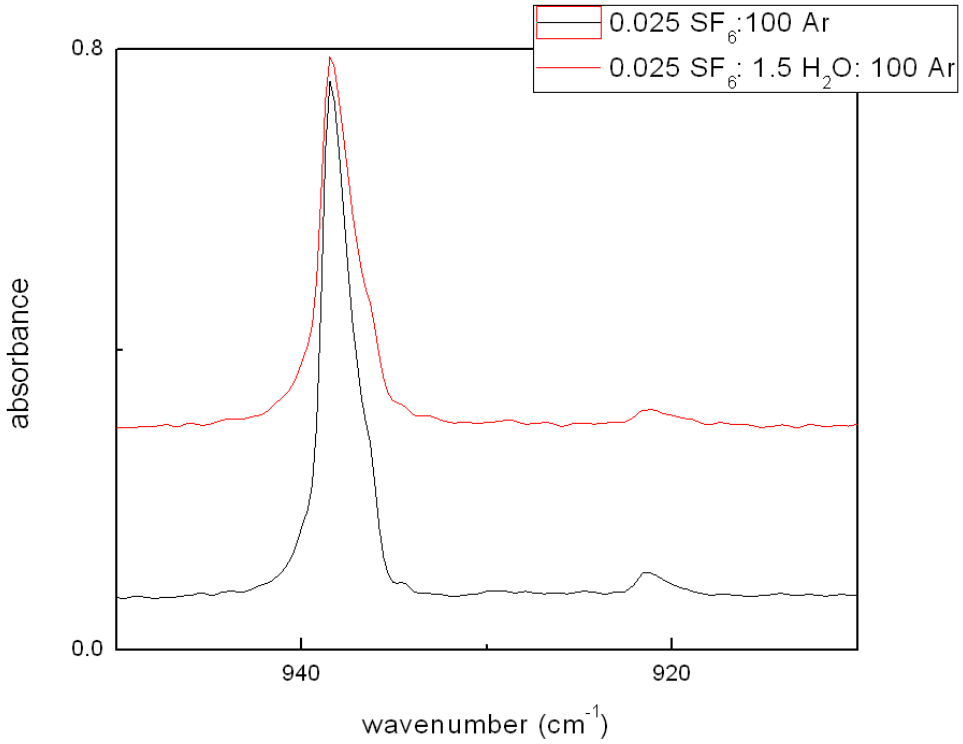

Figure 16: Low Concentration SF_6 studies

Additionally, these trials were subjected to an annealing process, which involves heating the matrix slightly from 6K to 25K. Annealing, theoretically, could allow the component molecules to move around within the solid argon matrix. This type of study could have two effects: 1) the complex which was formed originally within the matrix is broken apart and peaks resulting from the complex decrease in size or disappear altogether as complex concentration decreases or 2) the movement of the molecules allows previously uncomplexed water and SF_6 molecules to find and interact with each other causing an increase or appearance of peaks resulting from the complex. It is difficult to predict the effects annealing would have but if either one of those two possibilities were to occur it would help solidify the classification of a peak believed to result from the H_2O-SF_6 complex.

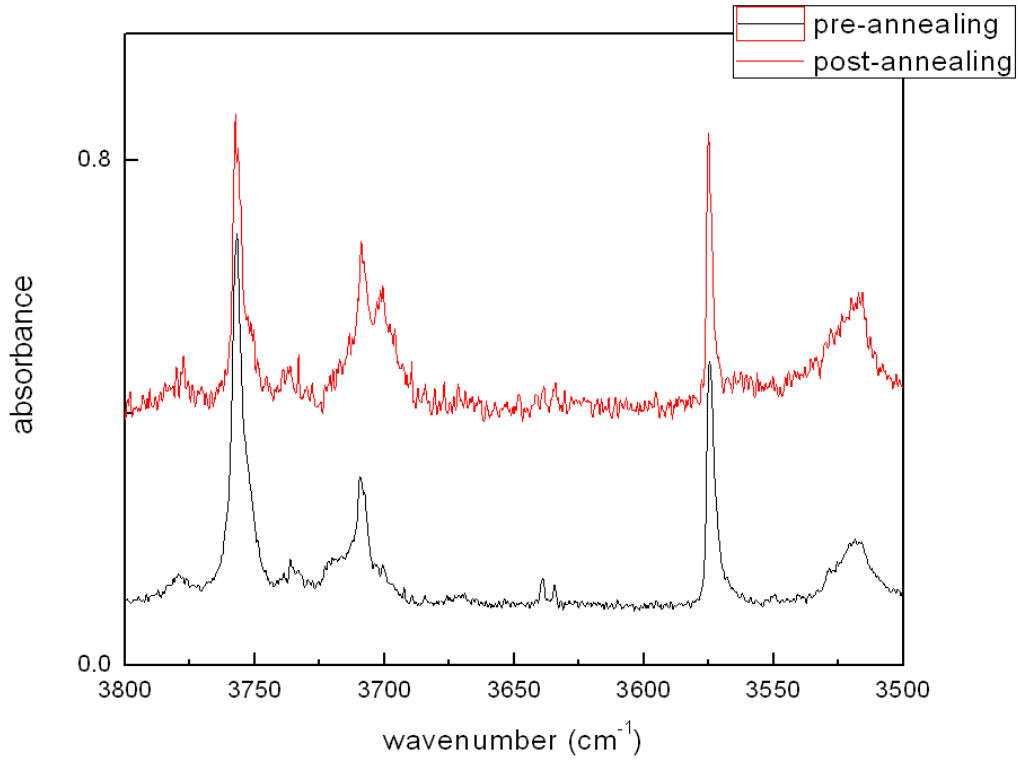
pre-annealing
post-annealing
absorbance
0.8
0.0
3800
3750
3700
3650
3600
3550
3500
wavenumber (cm-1)

a)

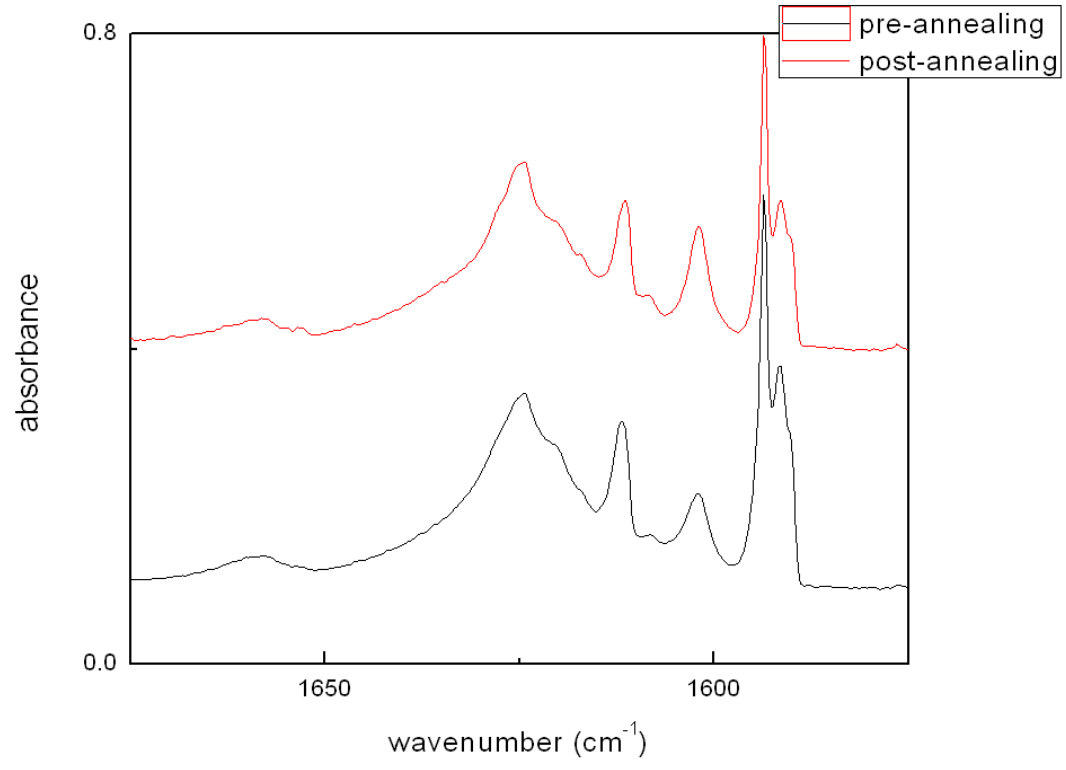
pre-annealing
post-annealing
absorbance
0.8
0.0
1650
1600
wavenumber (cm-1)

b)

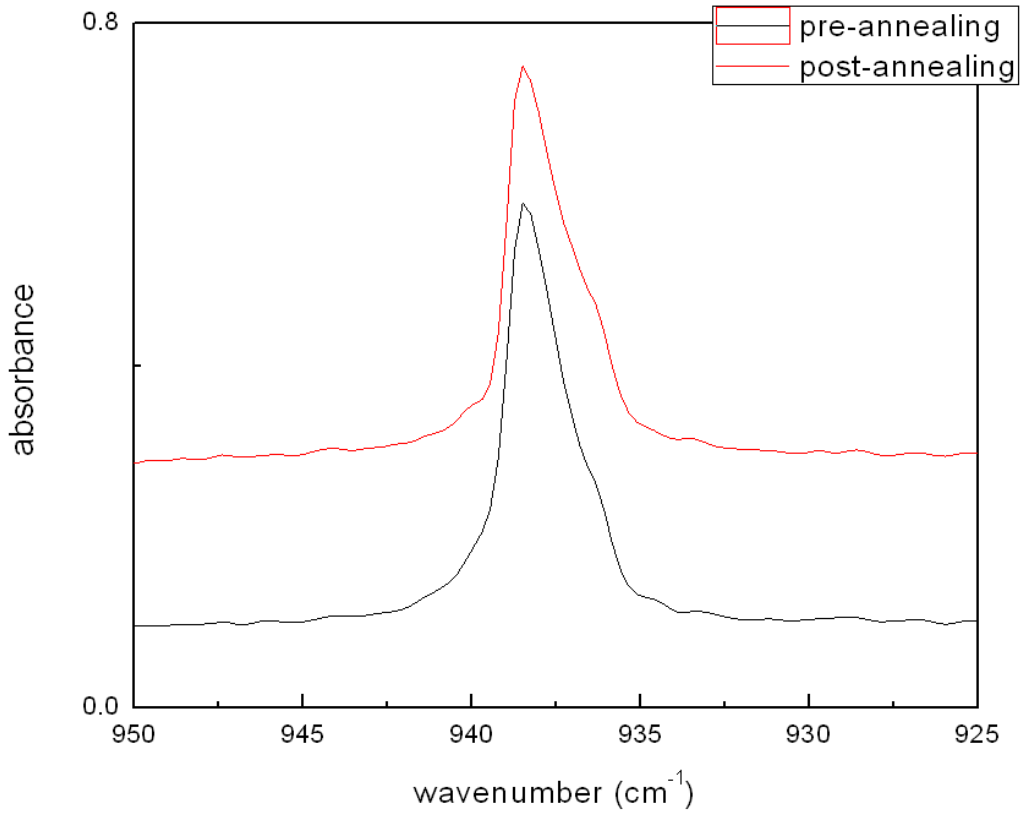

c)

Figure 17: Effect of Annealing at 25K for 10 minutes (0.025 SF_6:1.5 H_2O:100 Ar)

From the annealing studies, it was noted that a two small shoulder peaks begin to form at approximately 933cm^{-1} and 941cm^{-1}. The peaks are not clearly distinguishable from the larger peak itself centered at 938cm^{-1}. However, since these trials did successfully decrease the relative abundance of the center peak to less than 1, the peaks could be analyzed using a Gaussian deconvolution method. Deconvolution is simply a means of "breaking down" a raw data spectrum by looking at peaks as a sum of Gaussian curves. Therefore, if these shoulder peaks could only be explained by additional Gaussian curves not present in the pre-annealing spectrum it would be possible they were due to

formation of the H_2O-SF_6 complex. To start, the spectrum was fitted using two peaks as the basis of the center, main peak in the spectrum.

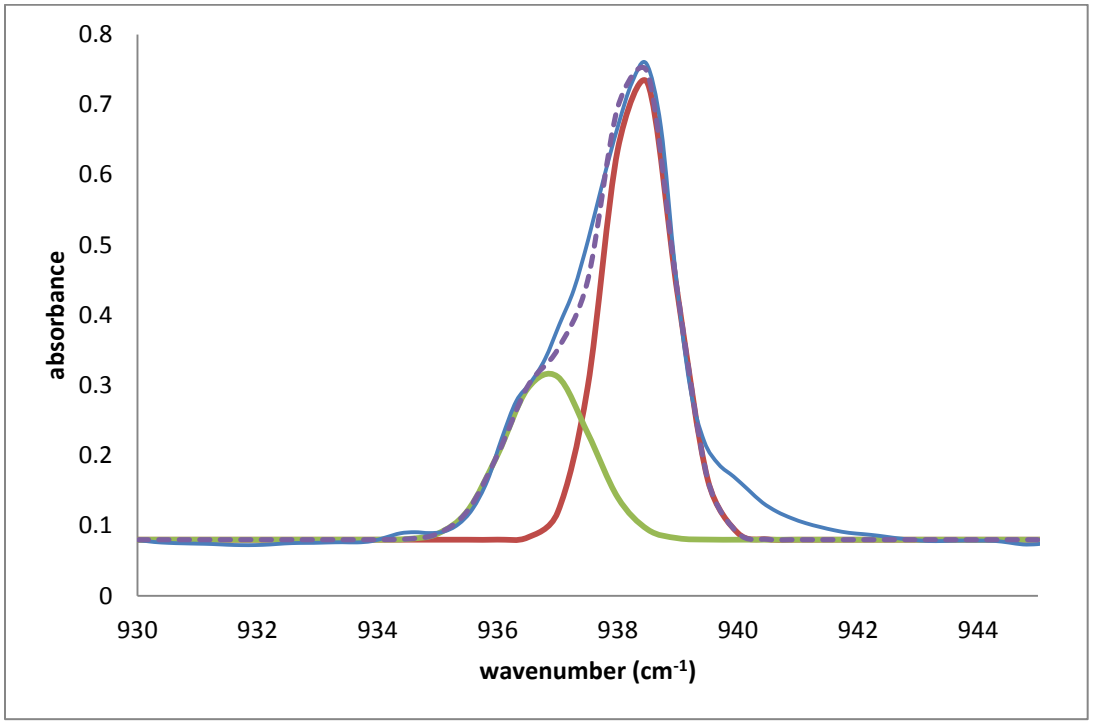

Figure 18: Gaussian Deconvolution of 0.025: 100 SF_6:Ar spectrum utilizing Two Base Peaks

Figure 18 clearly depicts that this particular peak in the spectrum cannot easily be fitted utilizing two base peaks. A small shoulder region exists around 940 cm^{-1} while only using two Gaussian curves as the base of this peak. In order to account for this shoulder region, a third peak had to be added.

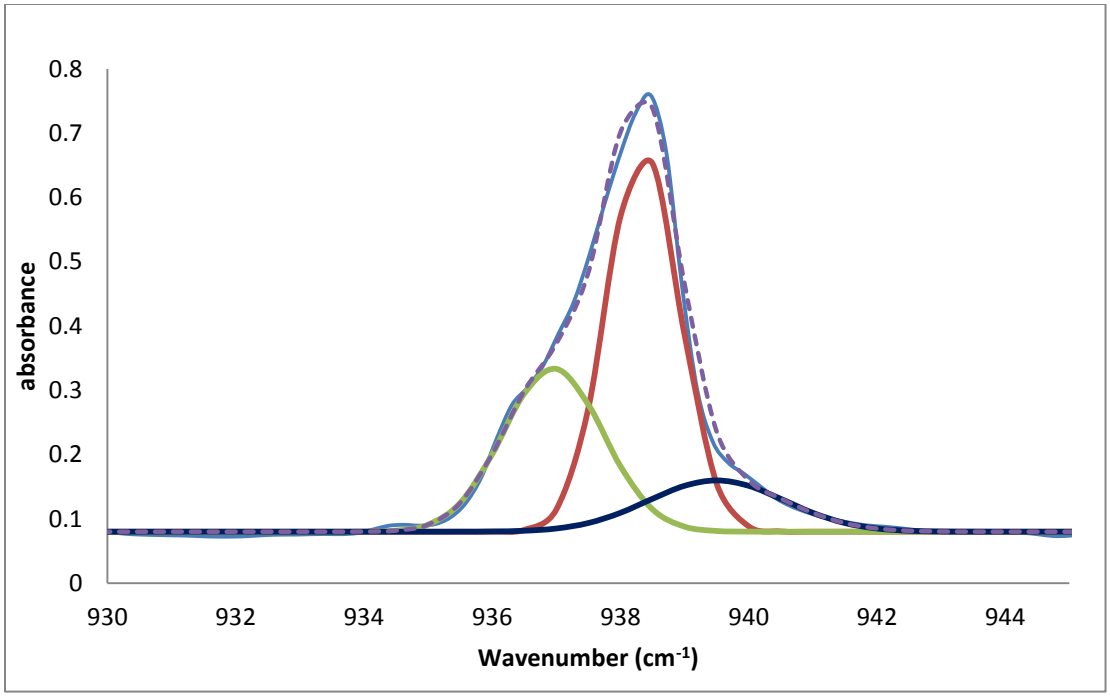

Figure 19: Gaussian Deconvolution of 0.025: 100 SF_6:Ar spectrum utilizing Two Base Peaks with an Additional Shoulder Peak

Exploiting three peaks instead of only two allows the full peak in the raw data spectrum to be explained as indicated by the close fit of the sum of the three Gaussian curves. Now this same fitting method was applied to the pre-annealing and post-annealing spectra of the 0.025 SF_6: 1 H_2O: 100 Ar mixture. If the pre-annealing spectrum can be closely fitted using a similar method to the SF_6 spectrum and the post-annealing spectrum requires additional peaks not present in the pre-annealing spectrum, then it would provide evidence that this peak could be a result of the formation of H_2O-SF_6 complex.

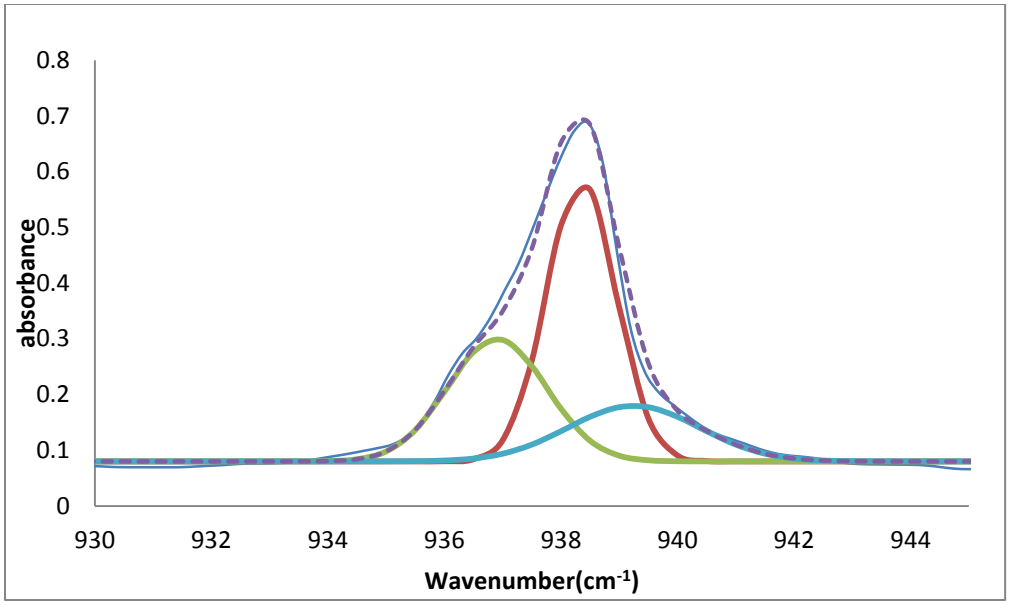

Figure 20: Gaussian Deconvolution of pre-annealing 0.025 SF_6:1 H_2O:100 Ar spectrum

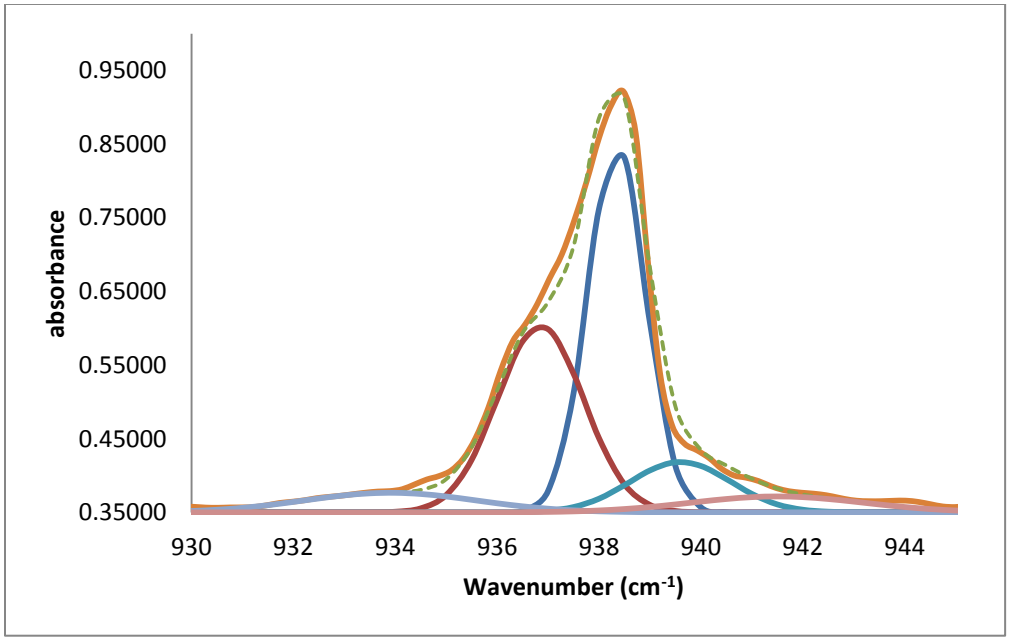

Figure 21: Gaussian Deconvolution of post-annealing 0.025 SF_6:1 H_2O:100 Ar spectrum

The two shoulder peaks centered around 934 cm^{-1} and 941.5 cm^{-1} are present in Figure 21 but not in Figure 20. These two peaks agree with shifts calculated with GAUSSIAN and correlate closely to the -5cm^{-1} and +1cm^{-1} shift displayed in Table 5. Based on this promising new evidence, several trials of the same concentration were carried out in order to ensure that this phenomenon was a repeatable occurrence. The Gaussian curving fitting graphs as well as the spectra for these trials can be found in the appendix. Those repeat trials also show the same result and support that those peaks are repeatable experimentally and that they show promise as being classified as peaks due to the H_2O-SF_6 complex.

However, previous SF_6 trials had not been subjected to the annealing process. Therefore, in order to rule out that these additional shoulder peaks in Figure 21 are not simply due to aggregation of SF_6 molecules, a sample of SF_6 was subjected to the annealing process.

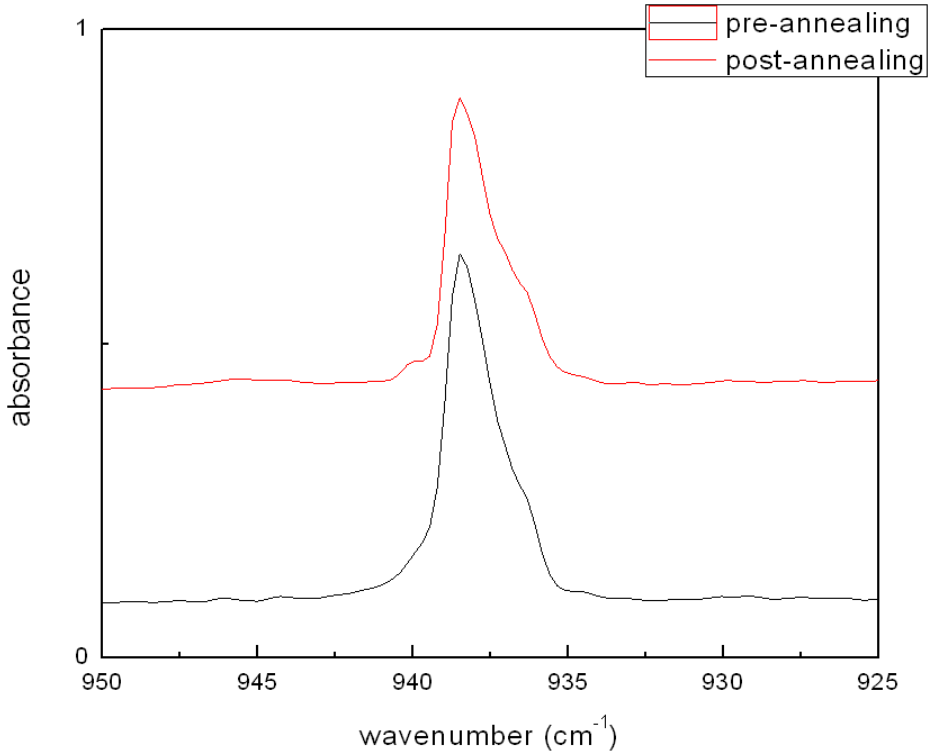

Figure 22: Spectrum of 0.025 SF_6: 100 Ar prior to annealing at 25K for 10 minutes and post-annealing

The raw spectrum of the post-annealing SF_6 trial does not appear to show the same shoulder peaks as demonstrated in the spectra of the H_2O and SF_6 mixture trials. Nevertheless, the same Gaussian deconvolution method was applied to this data as well.

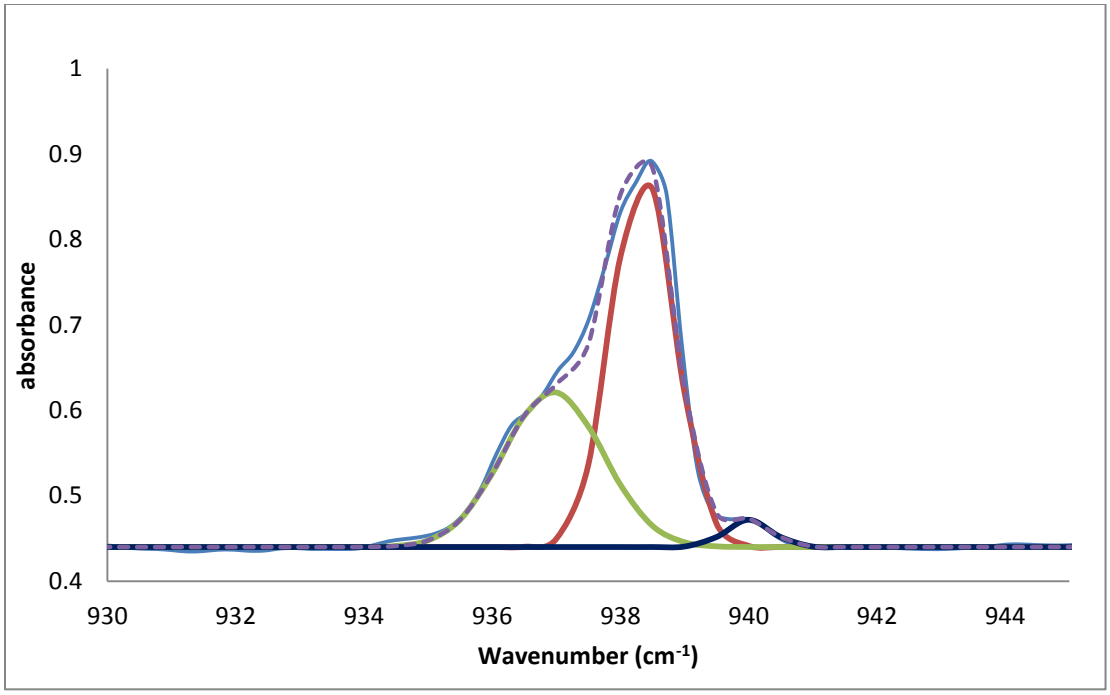

Figure 23: Gaussian curve fitting of 0.025 SF_6: 100 Ar post-annealing at 25K for 10 minutes

There does not seem to be the same shoulder peak pattern shown here for the annealed SF_6 alone as there was for the annealed mixture. The shoulder peak around 940cm^{-1} does appear to be shifted as is the case with the other annealed mixtures, but the peak around 933cm^{-1} is absent. The Gaussian deconvolution of the peaks in question as well as the annealing of the SF_6 trial demonstrate a case for the classification of these peaks resulting from the H_2O-SF_6 complex. It does seem slightly counter-intuitive that the annealing process would have this effect on a complex with such a weak interaction as that of water and SF_6. Initially it would seem that the annealing process would more likely break apart existing H_2O-SF_6 dimers causing the peak height to decrease. Not to

say that annealing would cause the migration of the molecule to come in closer proximity is completely out of the question, it just seems far more unlikely. In any case, the Gaussian curve fitting show that there are, in fact, peaks that are both repeatable and not explainable by the annealing process of SF_6 alone. Based on this data, it cannot be proven beyond a shadow of a doubt that these peaks are a result of the complex, but that fact has not been disproven either. Nonetheless, the assignments based on this deconvolution are weak and would not be able to stand on their own. While the case presented so far makes it reasonable to state that those peaks are due to the complex, it is not an assignment made with absolute certainty.

In order to provide more validity to the argument present above for the assignment of the shoulder peaks at 934cm^{-1} and 941.5cm^{-1}, the search began for another candidate peak that would also match up with the theoretical GUASSIAN calculations. With all of the other candidate regions thoroughly searched, the final region that held a promising shift in the GAUSSIAN calculation was the SF_6 peak around 630cm^{-1} with a shift of approximately -4cm^{-1}. This peak in the experimental spectrum occurs around 612cm^{-1}, very close to the edge of the observable range of the FTIR instrument being used. Despite this fact, this range was searched for candidate peaks that were distinguishable from the noise associated with approaching the range limit of the spectrometer. One such candidate peak was found as a shoulder peak off the main peak at 612cm^{-1}.

The candidacy of the peak in question was further analyzed by carrying out a concentration study, where the concentration of SF_6 was held constant as the concentration of water was increased. Again, this concentration study would have the same effect as the SF_6 concentration studies discussed previously. However, in this case altering the SF_6 concentration would not prove or disprove the possibility of this as a complex peak since the peak would increase if it were only due to SF_6 as well. Water does not have any IR active motions that absorb in this region of the spectrum, so if increasing the water concentration, while holding SF_6 concentration constant, causes the peak in question to increase absorbance, then it is most likely due to the H_2O-SF_6 complex.

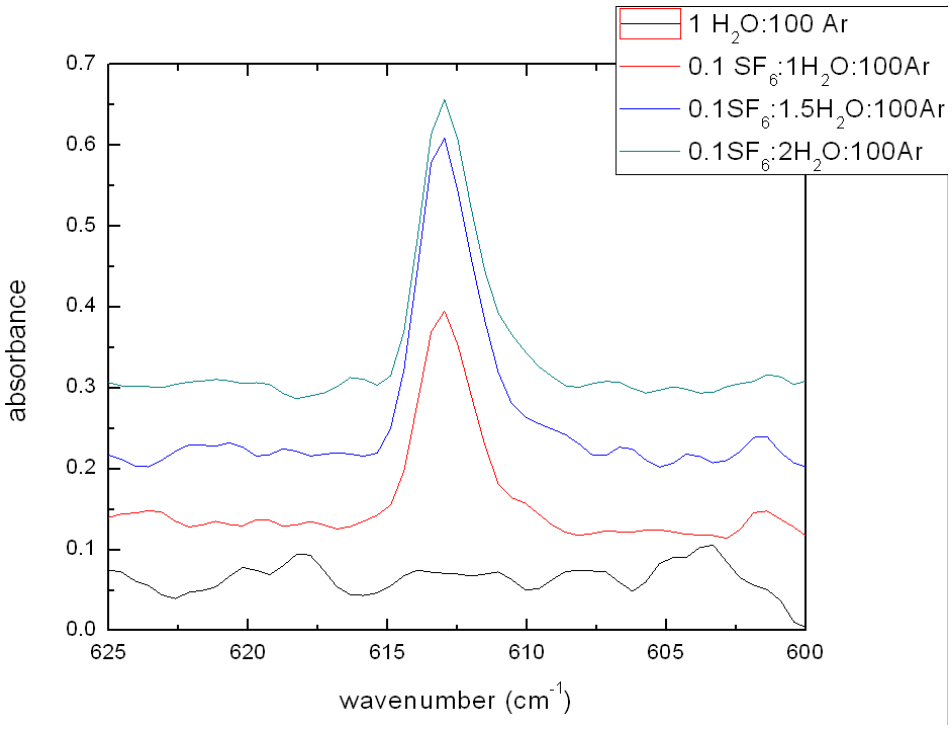

Figure 24: Water concentration studies

The candidate peak at approximately 608cm^{-1} does appear to have some correlation to the increase in water concentration, this fact, combined with the close correlation of the shift to one theoretically calculated for the H_2O-SF_6 complex, makes a strong case for this peak to be a result of the complexation of SF_6 with water. However, further studies would need to be conducted in order to ensure that this phenomenon is not simply an artifact of the noise in this region.

CONCLUSION

In conclusion, the research described here was aimed at theoretically calculating the expected shifts of the IR absorption bands of SF_6 upon complexation with water and to find experimental evidence of the H_2O-SF_6 complex. The theoretical calculations showed that the hydrogen atoms of the water molecule coordinate with the fluorine atoms of the SF_6 molecule. The very shallow potential energy surface which describes the dimer, leads to the possibility that the nature of the interaction is not an actual hydrogen bond, as was once previously believed with NF_3. Despite the weak interaction, the GAUSSIAN calculations did show that there would be shifts in the absorption bands that could be observed experimentally.

The shift in the H_2O bending region proved much too small to reliably detect experimentally at a value of approximately -0.10cm^{-1}. The theoretically calculated shift in the H_2O stretching region did appear to be a plausible place to begin the search for a candidate H_2O-SF_6 peak due to the large shift of around 10cm^{-1}. If such a peak did exist it remained elusive in the spectra obtained. The original non-rotating monomer peak of water in this region (3736cm^{-1}) is very small to begin with and the amount of complex formed would only produce a peak at a fraction of that already small intensity. Therefore, the search for an H_2O-SF_6 complex peak in this region was unsuccessful as well.

Since the search for candidate peaks in the water absorbing regions previously utilized by the search for H_2O-NF_3 peaks proved ineffective, the investigation then turned to the SF_6 absorbing region. The results from the calculations in this region also proved promising with calculated shifts off the most intense peak of nearly -5cm^{-1} and +1cm^{-1}, both of which should be experimentally observable. This search revealed in two possible candidate peaks in the form of shoulder peaks off the peak at 938cm^{-1} as a result of the annealing process. Further classification of these peaks required the process of Guassian deconvolution, or fitting, where Gaussian curves are fitted to the raw data spectrum. This analysis did in fact reveal that those two shoulder peaks most likely were not present in the pre-annealing spectrum. Additional studies of SF_6 only annealing indicated that this same pattern of shoulder peaks is not reproducible through aggregation of SF_6 molecules alone. Therefore, it is possible that the annealing allowed the migration of H_2O and SF_6 molecules through the matrix and caused an increase in the concentration of the complex. Although, this result is counter-intuitive based on the very shallow potential energy surface of the complex, it does indicate the possibility that these two shoulder peaks could be caused the complexation of SF_6 with water.

In order to provide supplementary evidence of the H_2O-SF_6 complex, the region of the second strongest intensity band of SF_6 was investigated. This region was not originally investigated due to its proximity to the capable wavelength region of the spectrometer. However, this region did show promising shifts theoretically and thus required further examination. A shoulder peak could be identified off the main peak at

612cm^{-1} in the spectrum of water and SF_6 that was not present in the spectrum of only SF_6 at the same concentration. Concentration studies, where the amount of water added to the mixture was increased, revealed a slight increase in this shoulder peak's intensity that was consistent with an increasing concentration of complex.

Although the initial candidate peaks around 934cm^{-1} and 941.5cm^{-1} would alone provide a weak argument, at best, for the identification of complex, the additional evidence provided by the shoulder peak around 608cm^{-1} makes the argument as a whole much more convincing. Additional studies would be required to say with 100% certainty these peaks are the result of the H_2O-SF_6 complex. A spectrometer with greater resolution than 0.5cm^{-1} could be utilized to in order to more fully resolve the shoulder peak around 608cm^{-1} and gas phase experiments would be able to investigate the shoulder peaks at 934cm^{-1} and 941.5cm^{-1} more thoroughly. Even though this research did not prove the presence of the H_2O-SF_6 complex, it did not disprove its existence either. Additionally, it has provided a strong base off of which further experimentation could potentially identify the complex.

APPENDIX 1A: Theoretical Calculations with B3LYP Calculation Method

Water Vibrational Frequencies by basis set

631G	631G++	6311G++	aug-cc-pVDZ	aug-cc-pVTZ
1678.65 (66.85)	1627.23 (78.33)	1640.48 (70.95)	1618.63 (71.33)	1616.88 (102.26)
3808.95 (1.75)	3815.10 (6.06)	3819.89 (7.48)	3794.51 (4.06)	3782.49 (18.22)
3915.51 (23.88)	3926.41 (56.52)	3921.16 (61.44)	3904.38 (60.62)	3871.27 (107.25)

Water bond angles

631G: 103.42
631G++:105.00
6311G++:105.06
aug-cc-pVDZ:104.75
aug-cc-pVTZ:104.57

SF_6 Vibrational Frequencies by basis set

631G	631G++	6311G++	aug-cc-pVDZ	aug-cc-pVTZ
314.74 (0.00)	307.20 (0.00)	321.17 (0.00)	310.13 (0.00)	325.18 (0.00)
314.74 (0.00)	307.20 (0.00)	321.17 (0.00)	310.13 (0.00)	325.18 (0.00)
314.74 (0.00)	307.20 (0.00)	321.17 (0.00)	310.13 (0.00)	325.18 (0.00)
484.72 (0.00)	474.96 (0.00)	486.91 (0.00)	457.77 (0.00)	489.83 (0.00)
484.72 (0.00)	474.96 (0.00)	486.91 (0.00)	457.77 (0.00)	489.83 (0.00)
484.72 (0.00)	474.96 (0.00)	486.91 (0.00)	457.77 (0.00)	489.83 (0.00)

565.95 (19.30)	557.16 (19.71)	572.43 (17.30)	550.01 (21.39)	573.42 (49.25)
565.95 (19.30)	557.16 (19.71)	572.43 (17.30)	550.01 (21.39)	573.42 (49.25)
565.95 (19.30)	557.16 (19.71)	572.43 (17.30)	550.01 (21.39)	573.42 (49.25)
627.25 (0.00)	596.53 (0.00)	596.72 (0.00)	617.90 (0.00)	605.29 (0.00)
627.25 (0.00)	596.53 (0.00)	596.72 (0.00)	617.90 (0.00)	605.29 (0.00)
712.19 (0.00)	689.07 (0.00)	703.45 (0.00)	698.14 (0.00)	730.10 (0.00)
917.90 (328.36)	876.38 (395.73)	881.43 (416.44)	926.53 (384.39)	863.72 (572.97)
917.90 (328.36)	876.38 (395.73)	881.43 (416.44)	926.53 (384.39)	863.72 (572.97)
917.90 (328.36)	876.38 (395.73)	881.43 (416.44)	926.53 (384.39)	863.72 (572.97)

Dimer

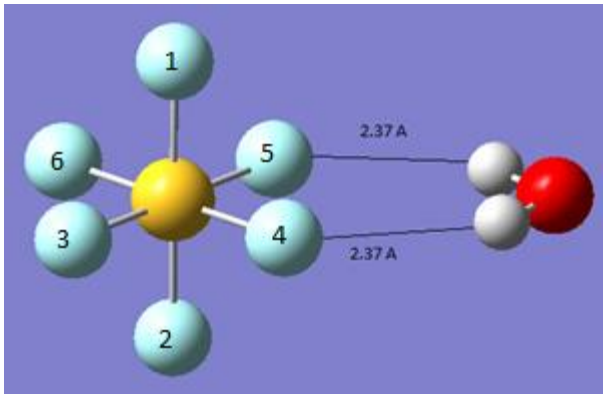

Water SF6_B3LYP_631G

Bond Angles

SF_6			
Angle Between Atoms	**Monomer**	**Dimer**	**Difference**
1-2	180.00	179.36	-0.64
1-3	90.00	90.22	0.22
1-4	90.00	89.77	-0.23
1-5	90.00	89.77	-0.23
1-6	90.00	90.22	0.22
2-3	90.00	90.22	0.22
2-4	90.00	89.77	-0.23
2-5	90.00	89.77	-0.23
2-6	90.00	90.22	0.22
3-4	90.00	89.90	-0.10
4-5	90.00	89.75	-0.25
5-6	90.00	89.90	-0.10
3-6	90.00	90.45	0.45
3-5	180.00	179.65	-0.35
4-6	180.00	179.65	-0.35
Water			
	104.57	102.90	-1.67

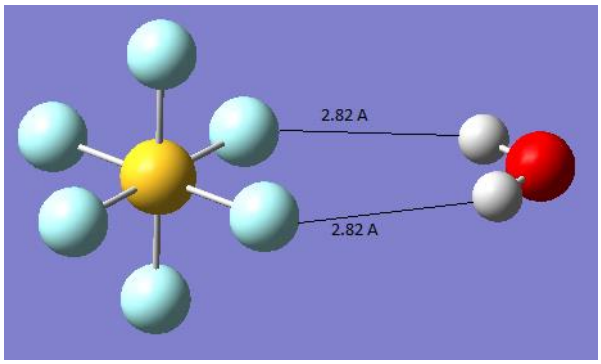

Water SF6_B3LYP_631G++

Bond Angles (same numbering scheme as above)

SF_6			
Angle Between Atoms	**Monomer**	**Dimer**	**Difference**
1-2	180.00	179.57	-0.43
1-3	90.00	90.15	0.15
1-4	90.00	89.85	-0.15
1-5	90.00	89.85	-0.15
1-6	90.00	90.15	0.15
2-3	90.00	90.15	0.15
2-4	90.00	89.85	-0.15
2-5	90.00	89.85	-0.15
2-6	90.00	90.15	0.15
3-4	90.00	89.99	-0.01
4-5	90.00	89.70	-0.30
5-6	90.00	89.99	-0.01
3-6	90.00	90.31	0.31
3-5	180.00	179.69	-0.31
4-6	180.00	179.69	-0.31
Water			
	104.57	104.73	0.16

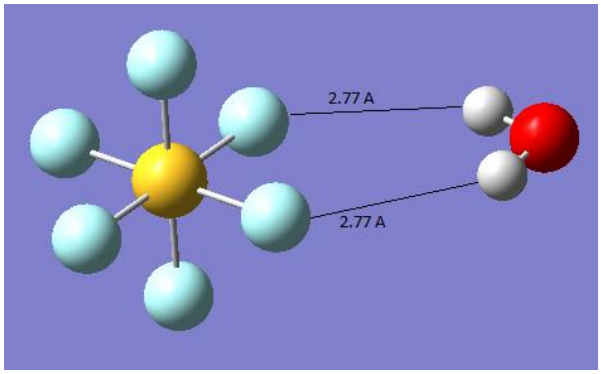

Water SF6_B3LYP_6311G++

Bond Angles

SF_6			
Angle Between Atoms	**Monomer**	**Dimer**	**Difference**
1-2	180.00	179.61	-0.39
1-3	90.00	90.14	0.14
1-4	90.00	89.86	-0.14
1-5	90.00	89.86	-0.14
1-6	90.00	90.14	0.14
2-3	90.00	90.14	0.14
2-4	90.00	89.86	-0.14
2-5	90.00	89.86	-0.14
2-6	90.00	90.14	0.14
3-4	90.00	89.98	-0.02
4-5	90.00	89.71	-0.29
5-6	90.00	89.98	-0.02
3-6	90.00	90.33	0.33
3-5	180.00	179.69	-0.31
4-6	180.00	179.69	-0.31
Water			
	104.57	104.87	0.30

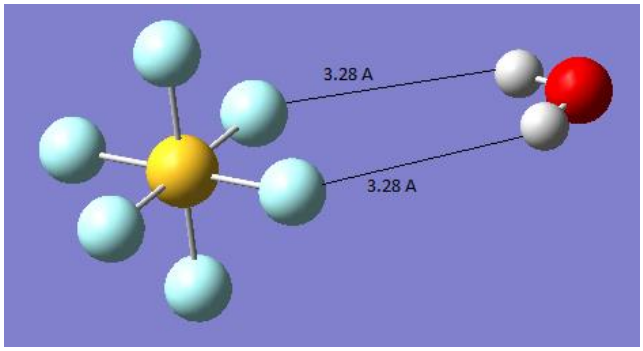

Water SF6_B3LYP_augccpVDZ

Bond Angles

SF_6			
Angle Between Atoms	**Monomer**	**Dimer**	**Difference**
1-2	180.00	179.98	-0.02
1-3	90.00	90.01	0.01
1-4	90.00	89.99	-0.01
1-5	90.00	89.99	-0.01
1-6	90.00	90.01	0.01
2-3	90.00	90.01	0.01
2-4	90.00	89.99	-0.01
2-5	90.00	89.99	-0.01
2-6	90.00	90.01	0.01
3-4	90.00	90.00	X
4-5	90.00	89.99	-0.01
5-6	90.00	90.00	X
3-6	90.00	90.02	0.02
3-5	180.00	179.99	-0.01
4-6	180.00	179.99	-0.01
Water			
	104.57	104.18	-0.39

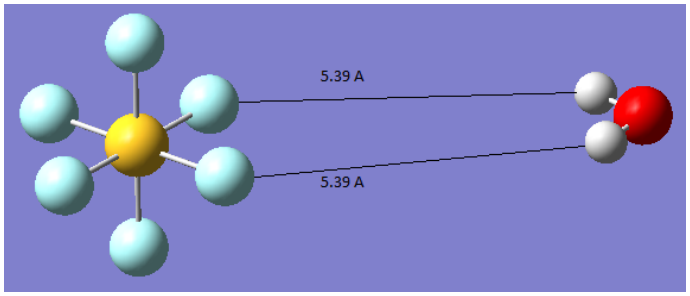

Water SF6_DFT_B3LYP_aug-cc-pVTZ

Bond Angles

SF_6			
Angle Between Atoms	**Monomer**	**Dimer**	**Difference**
1-2	180.00	180.00	X
1-3	90.00	90.00	X
1-4	90.00	90.00	X
1-5	90.00	90.00	X
1-6	90.00	90.00	X
2-3	90.00	90.00	X
2-4	90.00	90.00	X
2-5	90.00	90.00	X
2-6	90.00	90.00	X
3-4	90.00	90.00	X
4-5	90.00	90.00	X
5-6	90.00	90.00	X
3-6	90.00	90.00	X
3-5	180.00	180.00	X
4-6	180.00	180.00	X
Water			
	104.57	104.57	X

Vibrational Frequencies of DFT_B3LYP level of theory calculations by basis set

631G	**631G++**	**6311G++**	**aug-cc-pVDZ**	**aug-cc-pVTZ**
-31.79[a] (33.82)[b]	-84.73 (91.86)	-15.49 (3.74)	-131.22 (113.35)	-141.48 (110.46)
52.19 (8.08)	-59.47 (0.00)	5.65 (79.97)	-63.09 (0.00)	-83.25 (0.00)
58.29 (132.23)	-11.60 (3.11)	17.90 (12.40)	-11.45 (10.73)	-40.18 (319.03)
59.16 (0.00)	20.22 (0.03)	22.27 (0.00)	-10.99 (0.84)	-27.98 (0.00)
101.15	31.98	48.68	31.37	3.84

(76.87)	(0.14)	(0.18)	(0.01)	(0.00)
101.40	84.78	98.24	58.84	9.73
(0.59)	(198.88)	(201.98)	(302.48)	(0.00)
314.40	306.78	319.08	308.38	323.23
(0.00)	(0.00)	(0.01)	(0.00)	(0.00)
315.32	307.31	319.22	309.96	324.31
(0.10)	(0.02)	(0.03)	(0.01)	(0.00)
315.44	307.68	319.92	310.09	324.32
(0.09)	(0.00)	(0.00)	(0.00)	(0.00)
483.87	474.32	485.20	456.35	488.98
(0.13)	(0.03)	(0.05)	(0.00)	(0.00)
483.89	475.28	486.50	456.40	488.98
(0.03)	(0.00)	(0.00)	(0.00)	(0.00)
483.99	475.45	486.97	457.41	489.31
(0.00)	(0.01)	(0.04)	(0.00)	(0.00)
562.60	556.02	569.76	543.57	572.78
(21.99)	(21.82)	(19.44)	(44.98)	(47.69)
564.28	557.43	570.65	543.89	572.79
(19.98)	(20.76)	(17.93)	(43.82)	(47.73)
567.13	557.50	571.14	544.23	573.07
(15.89)	(17.94)	(15.14)	(42.58)	(48.65)
620.43	594.58	592.92	609.52	604.71
(0.30)	(0.23)	(0.38)	(0.00)	(0.00)
626.24	597.10	596.21	609.93	605.34
(1.62)	(0.54)	(0.71)	(0.00)	(0.00)
708.92	688.82	702.72	697.88	729.54
(1.44)	(0.53)	(0.78)	(0.00)	(0.00)
907.94	873.45	877.48	885.07	864.97
(388.01)	(374.15)	(457.25)	(555.90)	(573.81)
908.23	873.61	877.66	885.09	864.98
(301.43)	(432.85)	(392.86)	(549.71)	(573.15)
920.77	879.48	884.75	885.29	864.99
(327.17)	(394.14)	(415.42)	(551.74)	(574.22)
1682.20	1631.23	1643.39	1610.33	1616.99
(143.73)	(114.64)	(108.97)	(102.54)	(102.13)
3825.35	3816.62	3822.33	3782.69	3782.60
(8.56)	(7.91)	(9.80)	(18.13)	(18.28)
3923.61	3924.87	3921.55	3878.48	3871.35
(22.55)	(46.88)	(51.84)	(100.61)	(107.17)

a: vibrational frequency (cm^{-1})
b: intensity

APPENDIX 1B: Theoretical Calculations with WB97XD Calculation Method

Water Vibrational Frequencies by basis set

631G++	6311G++	cc-pVDZ	cc-pVTZ	Ultrafine-cc-pVTZ
1636.08 (82.20)	1646.07 (72.99)	1668.21 (60.30)	1645.51 (69.72)	1639.70 (97.96)
3905.03 (9.27)	3902.49 (9.43)	3854.97 (7.38)	3885.09 (4.54)	3872.04 (15.40)
4019.27 (4019.27)	4007.63 (65.91)	3960.00 (33.19)	3989.76 (45.31)	3962.91 (80.12)

Water bond angles

631G++: 105.13
6311G++: 105.21
cc-pVDZ: 102.99
cc-pVTZ: 104.61
ultrafine-cc-pVTZ: 104.10

SF_6 Vibrational Frequencies by basis set

631G++	6311G++	cc-pVDZ	cc-pVTZ	Ultrafine-cc-pVTZ
316.71 (0.00)	330.61 (0.00)	326.33 (0.00)	339.28 (0.00)	339.94 (0.00)
316.71 (0.00)	330.61 (0.00)	326.33 (0.00)	339.28 (0.00)	339.94 (0.00)
316.71 (0.00)	330.61 (0.00)	326.33 (0.00)	339.28 (0.00)	339.94 (0.00)
489.40 (0.00)	501.53 (0.00)	478.54 (0.00)	509.05 (0.00)	509.98 (0.00)
489.40 (0.00)	501.53 (0.00)	478.54 (0.00)	509.05 (0.00)	509.98 (0.00)

489.40 (0.00)	501.53 (0.00)	478.54 (0.00)	509.05 (0.00)	509.98 (0.00)
568.52 (53.55)	584.77 (48.14)	569.62 (56.40)	595.61 (56.32)	596.15 (54.28)
568.52 (53.55)	584.77 (48.14)	569.62 (56.40)	595.61 (56.32)	596.15 (54.28)
568.52 (53.55)	584.77 (48.14)	569.62 (56.40)	595.61 (56.32)	596.15 (54.28)
615.57 (0.00)	615.34 (0.00)	662.89 (0.00)	638.25 (0.00)	634.38 (0.00)
615.57 (0.00)	615.34 (0.00)	662.89 (0.00)	638.25 (0.00)	634.38 (0.00)
726.34 (0.00)	741.12 (0.00)	753.86 (0.00)	771.18 (0.00)	769.67 (0.00)
870.04 (570.18)	874.12 (584.47)	959.32 (527.15)	913.56 (580.56)	910.77 (582.26)
870.04 (570.18)	874.12 (584.47)	959.32 (527.15)	913.56 (580.56)	910.77 (582.26)
870.04 (570.18)	874.12 (584.47)	959.32 (527.15)	913.56 (580.56)	910.77 (582.26)

Dimer

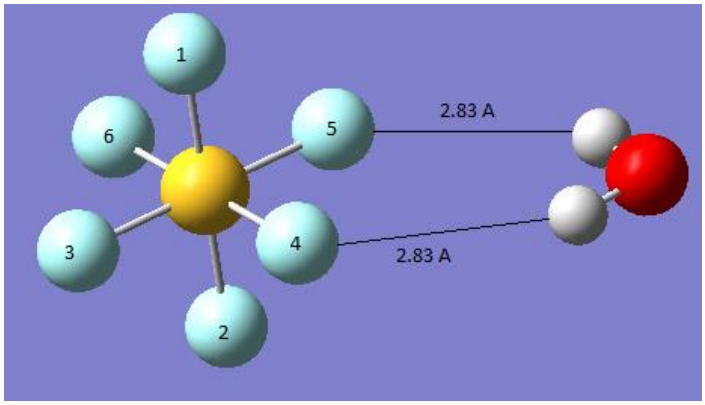

WaterSF6_DFT_WB97XD_631G++

Bond Angles

SF_6			
Angle Between Atoms	**Monomer**	**Dimer**	**Difference**
1-2	180.00	179.55	-0.45
1-3	90.00	90.16	0.16
1-4	90.00	89.84	-0.16
1-5	90.00	89.84	-0.16
1-6	90.00	90.16	0.16
2-3	90.00	90.16	0.16
2-4	90.00	89.84	-0.16
2-5	90.00	89.84	-0.16
2-6	90.00	90.16	0.16
3-4	90.00	89.98	-0.02
4-5	90.00	89.74	-0.26
5-6	90.00	89.98	-0.02
3-6	90.00	90.29	0.29
3-5	180.00	179.72	-0.28
4-6	180.00	179.72	-0.28
Water			
	104.10	104.84	0.74

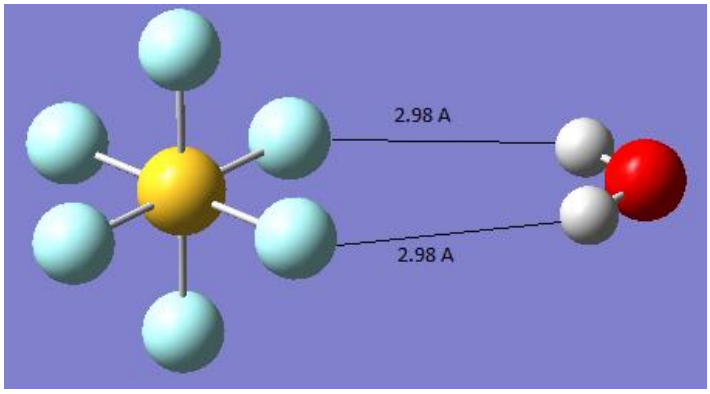

WaterSF6_DFT_WB97XD_6311G++
(same numbering of complex)

Bond Angles

SF_6			
Angle Between Atoms	**Monomer**	**Dimer**	**Difference**
1-2	180.00	179.94	-0.06
1-3	90.00	90.02	0.02
1-4	90.00	89.98	-0.02
1-5	90.00	89.98	-0.02
1-6	90.00	90.02	0.02
2-3	90.00	90.02	0.02
2-4	90.00	89.98	-0.02
2-5	90.00	89.98	-0.02
2-6	90.00	90.02	0.02
3-4	90.00	89.97	-0.03
4-5	90.00	90.01	0.01
5-6	90.00	89.97	-0.03
3-6	90.00	90.04	0.04
3-5	180.00	179.98	-0.02
4-6	180.00	179.98	-0.02
Water			
	104.10	104.69	0.59

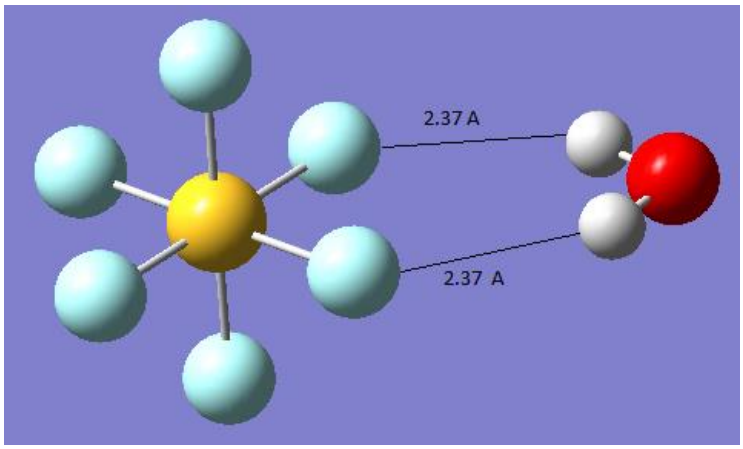

WaterSF6_DFT_WB97XD_ccpVDZ

Bond Angles

SF_6			
Angle Between Atoms	**Monomer**	**Dimer**	**Difference**
1-2	180.00	179.51	-0.49
1-3	90.00	90.17	0.17
1-4	90.00	89.83	-0.17
1-5	90.00	89.83	-0.17
1-6	90.00	90.17	0.17
2-3	90.00	90.17	0.17
2-4	90.00	89.83	-0.17
2-5	90.00	89.93	-0.17
2-6	90.00	90.17	0.17
3-4	90.00	89.94	-0.06
4-5	90.00	89.76	-0.24
5-6	90.00	89.94	-0.06
3-6	90.00	90.36	0.36
3-5	180.00	179.70	-0.30
4-6	180.00	179.70	-0.30
Water			
	104.10	102.34	-1.76

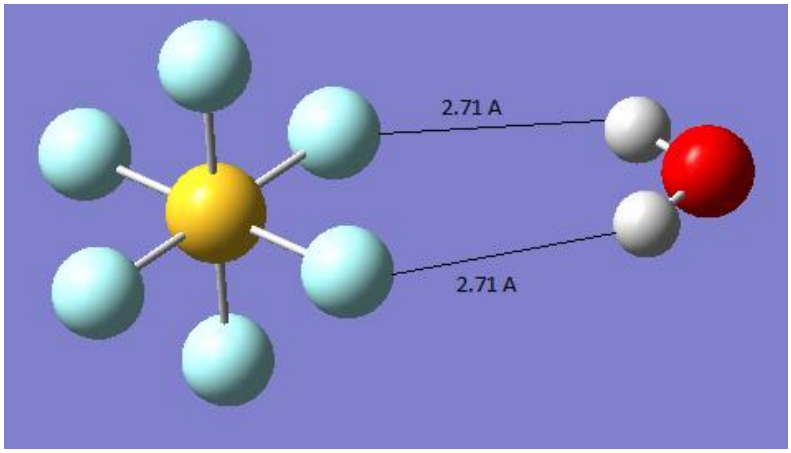

WaterSF6_DFT_WB97XD_ccpVTZ

Bond Angles

SF_6			
Angle Between Atoms	**Monomer**	**Dimer**	**Difference**
1-2	180.00	175.75	-0.25
1-3	90.00	90.09	0.09
1-4	90.00	89.91	-0.09
1-5	90.00	89.91	-0.09
1-6	90.00	90.09	0.09
2-3	90.00	90.09	0.09
2-4	90.00	89.91	-0.09
2-5	90.00	89.91	-0.09
2-6	90.00	90.09	0.09
3-4	90.00	89.96	-0.04
4-5	90.00	89.92	-0.08
5-6	90.00	89.96	-0.04
3-6	90.00	90.16	0.16
3-5	180.00	179.88	-0.12
4-6	180.00	179.88	-0.12
Water			
	104.10	104.23	0.13

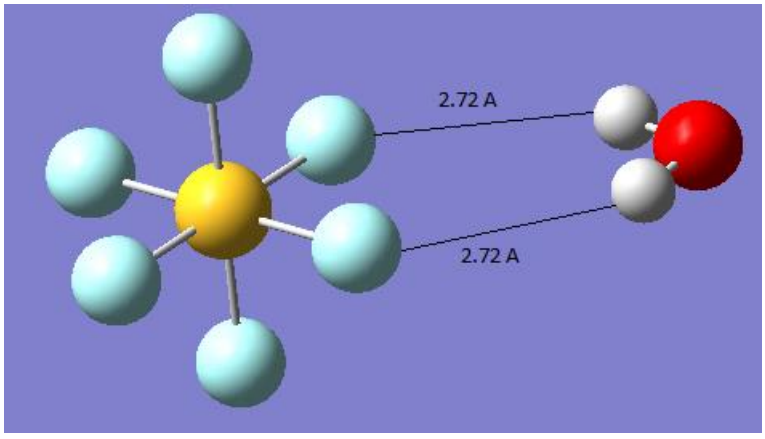

WaterSF6_DFT_WB97XD_ccpVTZ_ultrafine

Bond Angles

SF_6			
Angle Between Atoms	**Monomer**	**Dimer**	**Difference**
1-2	180.00	179.76	-0.24
1-3	90.00	90.08	0.08
1-4	90.00	89.91	-0.09
1-5	90.00	89.91	-0.09
1-6	90.00	90.08	0.08
2-3	90.00	90.08	0.08
2-4	90.00	89.91	-0.09
2-5	90.00	89.91	-0.09
2-6	90.00	90.08	0.08
3-4	90.00	89.97	-0.03
4-5	90.00	89.90	-0.10
5-6	90.00	89.97	-0.03
3-6	90.00	90.16	0.16
3-5	180.00	179.87	-0.13
4-6	180.00	179.87	-0.13
Water			
	104.10	104.25	0.15

Water-SF_6 Vibrational Frequencies by basis set- calculated using WB97XD level of theory

631G++	6311G++	cc-pVDZ	cc-pVTZ	Ultrafine-cc-pVTZ
-63.76 (88.07)	-156.88 (128.45)	-5.95 (3.18)	-135.47 (111.15)	-86.42 (71.84)
-19.33 (0.79)	-22.74 (0.01)	41.84 (25.67)	-34.40 (102.92)	-31.56 (117.52)
30.10 (6.86)	-18.44 (6.84)	85.57 (0.93)	54.70 (0.34)	58.18 (0.30)
37.50 (0.00)	18.90 (0.00)	109.78 (106.30)	64.25 (18.29)	64.27 (194.69)
40.26 (0.11)	51.91 (0.09)	118.88 (0.00)	67.85 (208.76)	88.76 (57.20)

110.81 (209.94)	80.21 (334.14)	124.27 (284.35)	89.00 (0.00)	93.24 (0.00)
317.31 (0.02)	328.61 (0.00)	324.71 (0.00)	337.51 (0.00)	338.30 (0.00)
317.38 (0.01)	328.79 (0.00)	326.78 (0.08)	338.45 (0.01)	339.15 (0.03)
317.86 (0.00)	329.51 (0.02)	327.48 (0.19)	338.83 (0.20)	339.43 (0.18)
490.82 (0.03)	501.09 (0.00)	478.16 (0.00)	508.62 (0.01)	509.35 (0.00)
491.19 (0.00)	501.39 (0.01)	478.18 (0.03)	508.63 (0.00)	509.36 (0.012)
491.28 (0.01)	502.20 (0.03)	478.49 (0.11)	509.83 (0.04)	509.71 (0.035)
574.98 (27.00)	583.52 (48.57)	567.67 (58.74)	594.58 (57.01)	595.37 (57.04)
575.80 (26.48)	584.14 (47.89)	568.41 (56.29)	595.62 (54.79)	596.11 (54.17)
576.26 (22.72)	585.33 (45.45)	570.43 (48.84)	596.83 (49.75)	597.21 (49.06)
624.08 (0.19)	615.55 (0.04)	658.67 (0.40)	635.68 (0.09)	630.29 (0.15)
625.46 (0.48)	616.20 (0.00)	663.58 (1.15)	637.98 (0.30)	634.47 (0.34)
728.42 (0.51)	743.29 (0.09)	754.00 (1.65)	771.44 (0.54)	768.31 (0.63)
915.83 (386.46)	873.75 (584.39)	957.03 (507.30)	913.37 (569.99)	904.93 (569.83)
915.85 (443.51)	878.16 (581.23)	957.91 (578.60)	914.04 (612.32)	905.70 (610.68)
916.79 (405.26)	878.32 (598.98)	963.99 (521.57)	915.83 (578.41)	911.87 (580.13)
1642.13 (114.93)	1646.54 (114.90)	1668.49 (126.41)	1636.20 (119.93)	1639.61 (199.69)
3907.91 (12.13)	3884.14 (28.35)	3860.36 (37.98)	3880.68 (21.37)	3880.85 (21.04)
4019.50 (53.05)	3976.33 (106.51)	3951.04 (60.49)	3973.51 (75.99)	3974.15 (76.76)

APPENDIX 2: Additional Gaussian curve fitting analyses

0.025 SF_6:100 Ar Replicate Trials

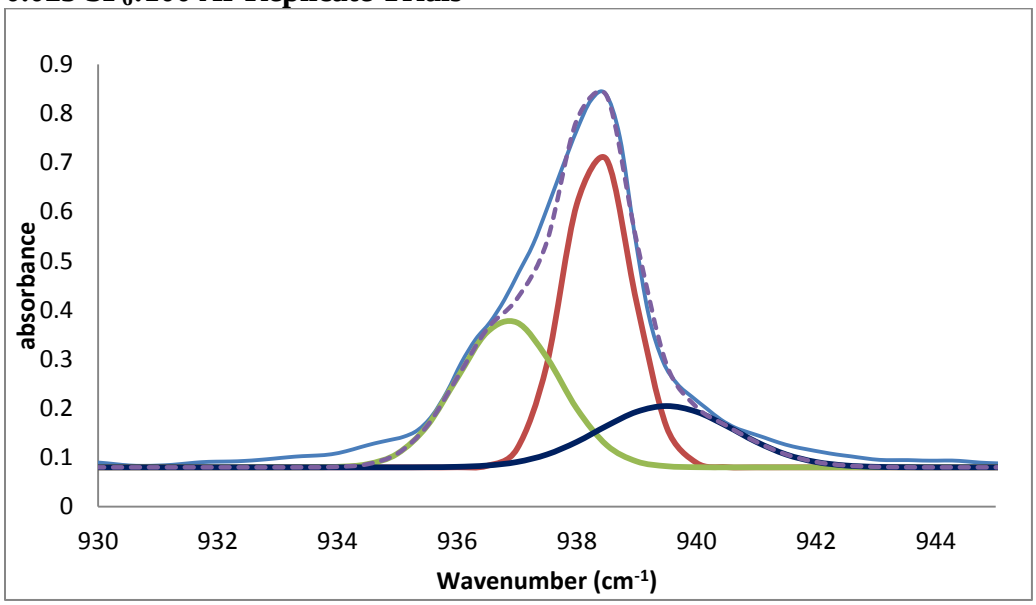

Trial 1: pre-annealing

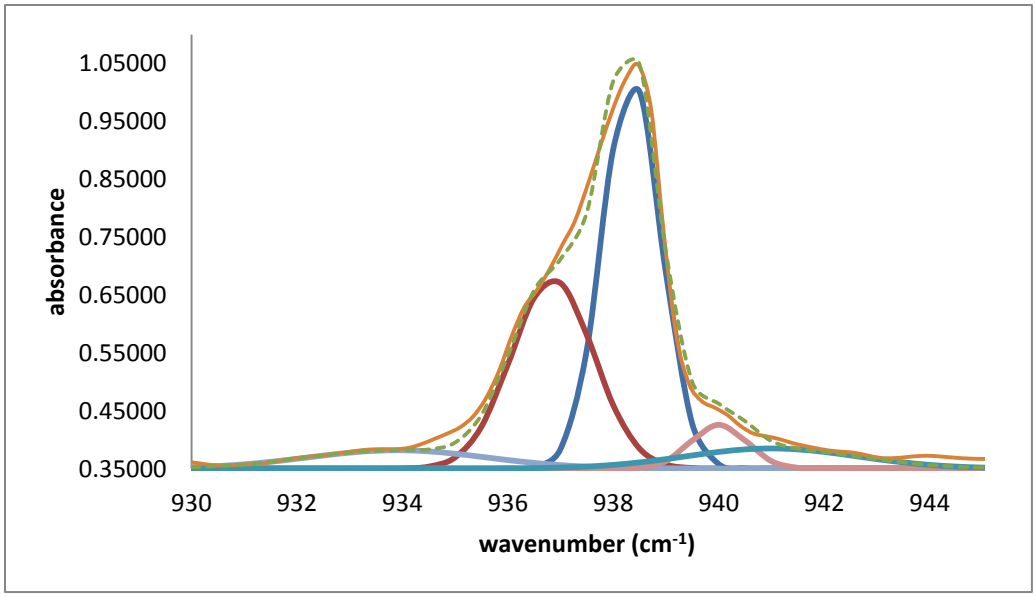

Trial 1: post-annealing

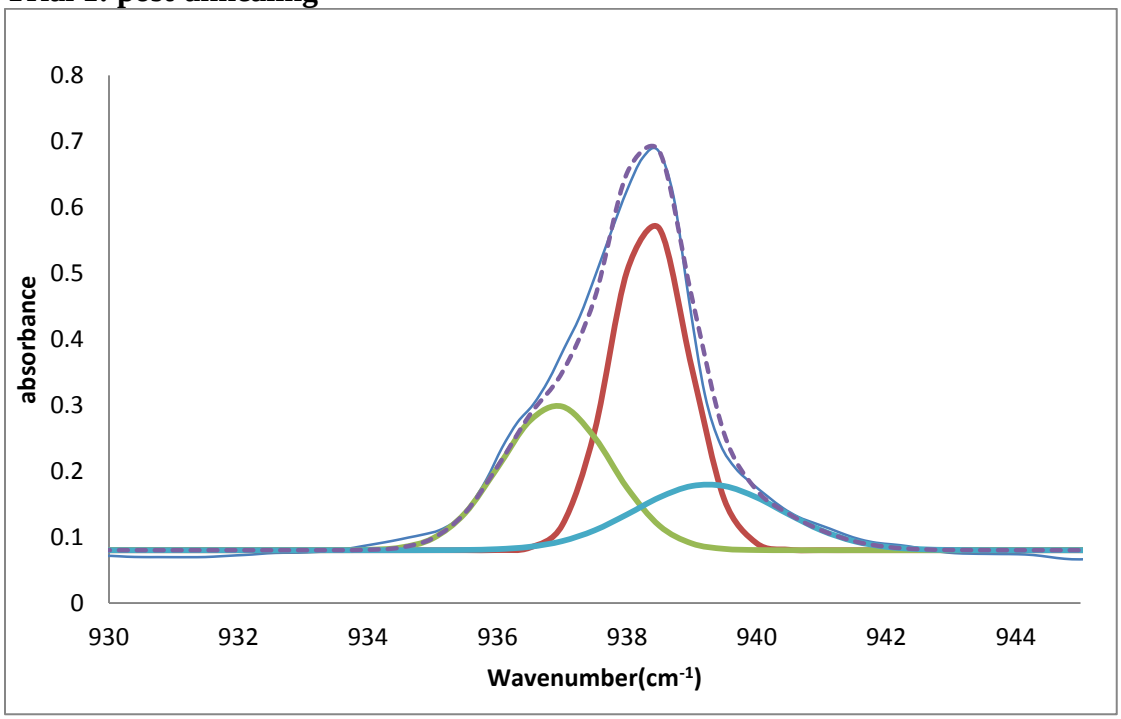

Trial 2: pre-annealing

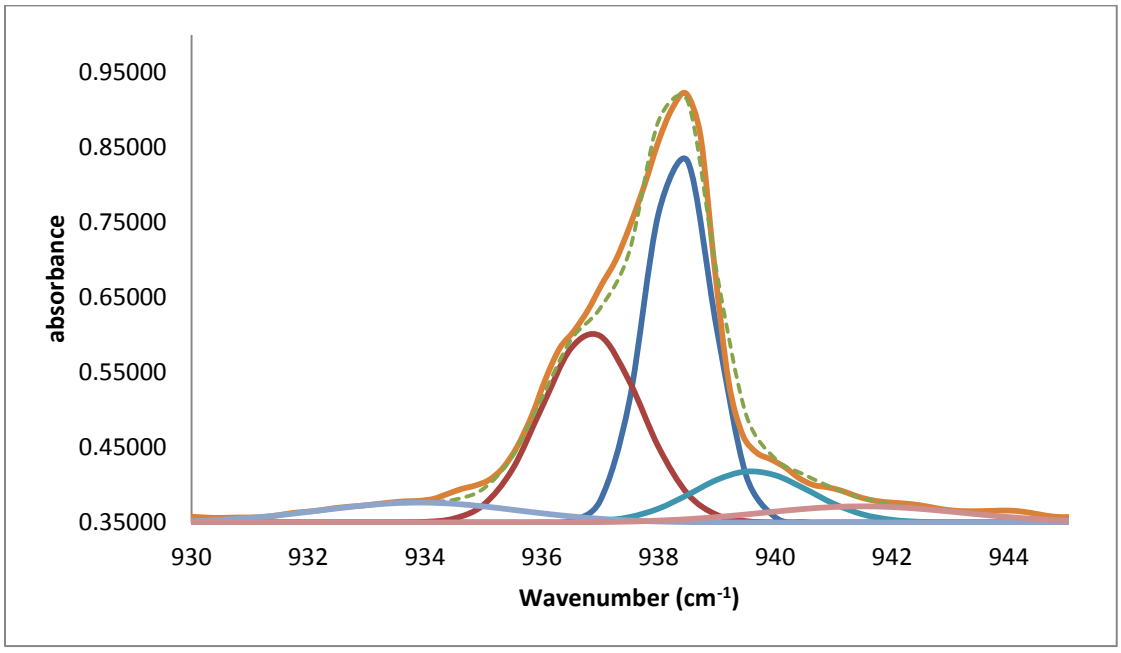

Trial 2: post-annealing

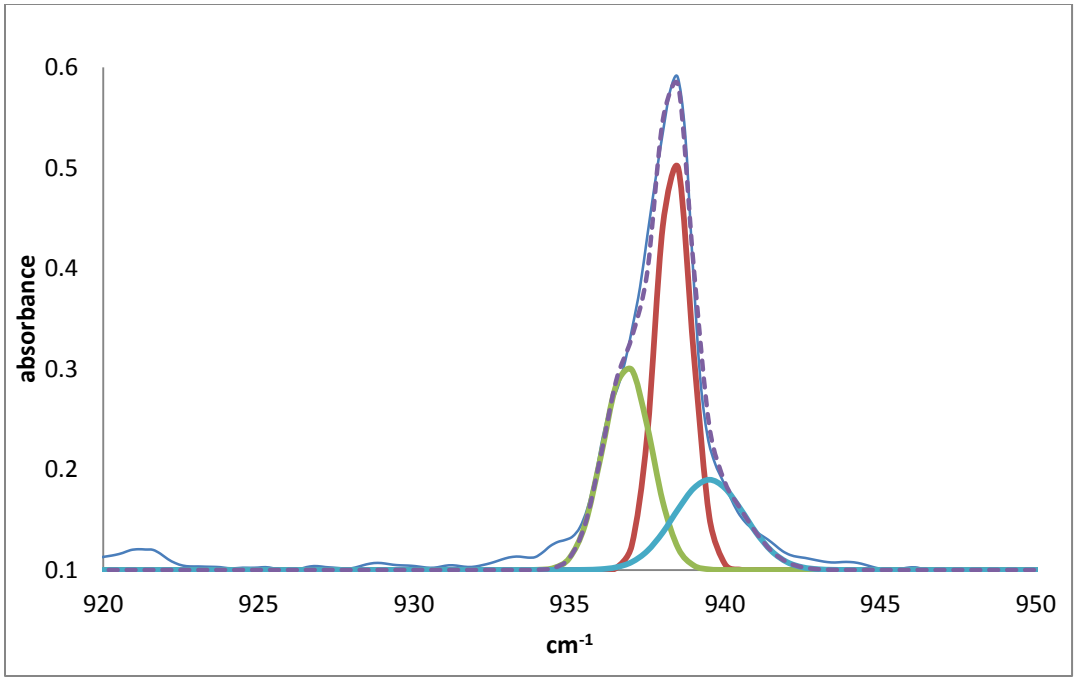

Trial 3: pre-annealing

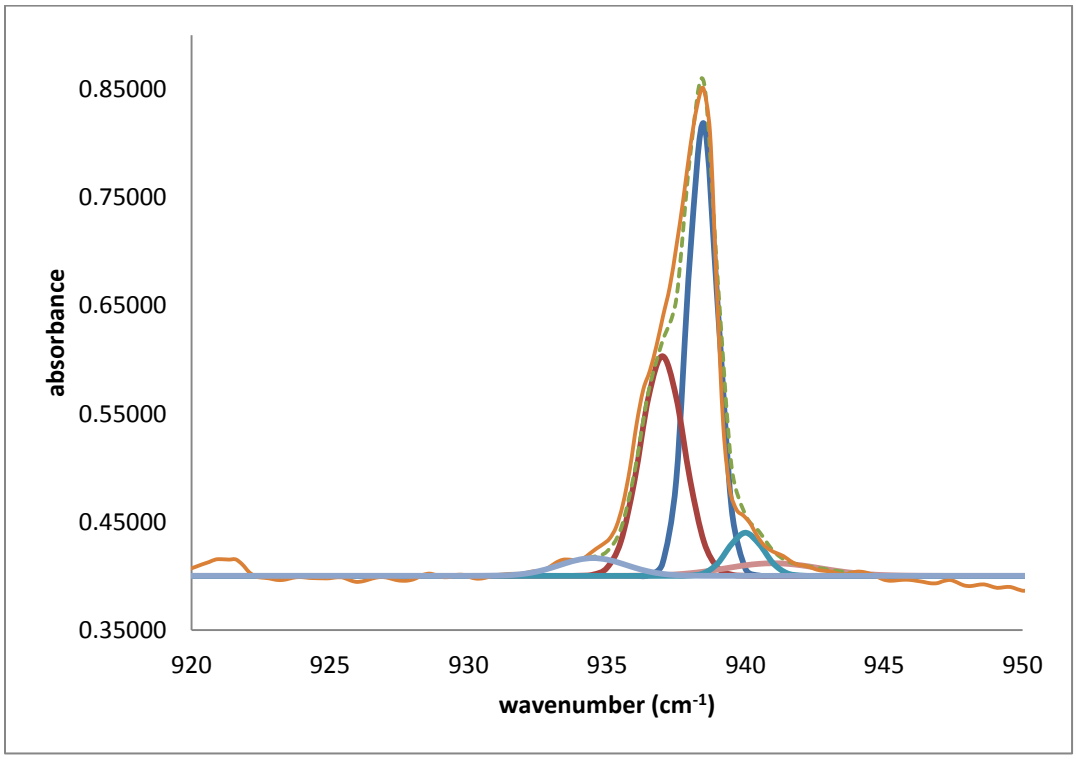

Trial 3: post-annealing

REFERENCES

1. NASA - Water Vapor Confirmed as Major Player in Climate Change. Available at: http://www.nasa.gov/topics/earth/features/vapor_warming.html. (Accessed: 17th December 2015)

2. Church, J. A. & White, N. J. A 20th century acceleration in global sea-level rise: AN ACCELERATION IN GLOBAL SEA-LEVEL RISE. *Geophys. Res. Lett.* **33,** (2006).

3. Triacca, U., Pasini, A., Attanasio, A., Giovannelli, A. & Lippi, M. Clarifying the Roles of Greenhouse Gases and ENSO in Recent Global Warming through Their Prediction Performance. *J. Clim.* **27,** 7903–7910 (2014).

4. Environmental Protection Agency -- Global Warming and Climate Change. Available at: http://www3.epa.gov/airtrends/aqtrnd95/globwarm.html. (Accessed: 16th February 2016)

5. Alain Tressaud. *Fluorine and the Environment: Atmospheric Chemistry, Emissions, & Lithosphere*. **1,** (Elsevier, 2006).

6. Maiss, M. & Brenninkmeijer, C. A. M. Atmospheric SF6: Trends, Sources, and Prospects. *Environ. Sci. Technol.* **32,** 3077–3086 (1998).

7. Zhang, J. *et al.* Decomposition of Potent Greenhouse Gas Sulfur Hexafluoride (SF6) by Kirschsteinite-dominant Stainless Steel Slag. *Environ. Sci. Technol.* **48,** 599–606 (2014).

8. US EPA, O. Basic Information| Polychlorinated Biphenyls (PCBs)| US EPA. Available at: http://www3.epa.gov/epawaste/hazard/tsd/pcbs/about.htm. (Accessed: 4th January 2016)

9. Reddmann, T., Ruhnke, R. & Kouker, W. Three-dimensional model simulations of SF6 with mesospheric chemistry. *J. Geophys. Res. Atmospheres* **106,** 14525–14537 (2001).

10. Arnold, T. *et al.* Nitrogen trifluoride global emissions estimated from updated atmospheric measurements. *Proc. Natl. Acad. Sci. U. S. A.* **110,** 2029–2034 (2013).

11. Montzka, S. A., Dlugokencky, E. J. & Butler, J. H. Non-CO2 greenhouse gases and climate change. *Nature* **476,** 43–50 (2011).

12. Dillon, T. J. *et al.* Removal of the potent greenhouse gas NF3 by reactions with the atmospheric oxidants O(1D), OH and O3. *Phys. Chem. Chem. Phys.* **13,** 18600–18608 (2011).

13. Weiss, R. F., Mühle, J., Salameh, P. K. & Harth, C. M. Nitrogen trifluoride in the global atmosphere. *Geophys. Res. Lett.* **35,** L20821 (2008).

14. It's Water Vapor, Not the CO2. *American Chemical Society* Available at: http://www.acs.org/content/acs/en/climatescience/climatesciencenarratives/its-water-vapor-not-the-co2.html. (Accessed: 6th January 2016)

15. Staikova, M. & Donaldson, D. J. Water complexes as catalysts in atmospheric reactions. *Phys. Chem. Earth Part C Sol. Terr. Planet. Sci.* **26,** 473–478 (2001).

16. Headrick, J. E. & Vaida, V. Significance of water complexes in the atmosphere. *Phys. Chem. Earth Part C Sol. Terr. Planet. Sci.* **26,** 479–486 (2001).

17. Scheiner, S. *Noncovalent Forces*. (Springer, 2015).

18. Dunitz, J. D. & Taylor, R. Organic Fluorine Hardly Ever Accepts Hydrogen Bonds. *Chem. – Eur. J.* **3,** 89–98 (1997).

19. Frank Weinhold and Roger Klein. What is a hydrogen bond? Resonance covalency in the supramolecular domain. *Chem Educ Res Pr.* **15,** 276–285 (2014).

20. Ian R. Dunkin. *Matrix Isolation Techniques: A Practical Approach*. (Oxford University Press, 1998).

21. Basis Sets. Available at: http://www.gaussian.com/g_tech/g_ur/m_basis_sets.htm. (Accessed: 31st January 2016)

22. Jolayna Wold. Identification of H2O-NF3 Complex in Argon Matrices.

23. M. J. Frisch, G. W. Trucks, H. B. Schlegel, G. E. Scuseria, M. A. Robb, J. R. Cheeseman, G. Scalmani, V. Barone, B. Mennucci, G. A. Petersson, H. Nakatsuji, M. Caricato, X. Li, H. P. Hratchian, A. F. Izmaylov, J. Bloino, G. Zheng, J. L. Sonnenberg, M. Hada, M. Ehara, K. Toyota, R. Fukuda, J. Hasegawa, M. Ishida, T. Nakajima, Y. Honda, O. Kitao, H. Nakai, T. Vreven, J. A. Montgomery, Jr., J. E.

Peralta, F. Ogliaro, M. Bearpark, J. J. Heyd, E. Brothers, K. N. Kudin, V. N. Staroverov, R. Kobayashi, J. Normand, K. Raghavachari, A. Rendell, J. C. Burant, S. S. Iyengar, J. Tomasi, M. Cossi, N. Rega, J. M. Millam, M. Klene, J. E. Knox, J. B. Cross, V. Bakken, C. Adamo, J. Jaramillo, R. Gomperts, R. E. Stratmann, O. Yazyev, A. J. Austin, R. Cammi, C. Pomelli, J. W. Ochterski, R. L. Martin, K. Morokuma, V. G. Zakrzewski, G. A. Voth, P. Salvador, J. J. Dannenberg, S. Dapprich, A. D. Daniels, Ö. Farkas, J. B. Foresman, J. V. Ortiz, J. Cioslowski, and D. J. Fox. *GAUSSIAN 09, Revision E.01*. (Gaussian, Inc., 2009).

24. Becke, A. D. Density-functional exchange-energy approximation with correct asymptotic behavior. *Phys. Rev. A* **38,** 3098–3100 (1988).

25. Becke, A. D. Density-functional thermochemistry. III. The role of exact exchange. *J. Chem. Phys.* **98,** 5648–5652 (1993).

26. Chai, J.-D. & Head-Gordon, M. Long-range corrected hybrid density functionals with damped atom-atom dispersion corrections. *Phys. Chem. Chem. Phys. PCCP* **10,** 6615–6620 (2008).

27. Nicholas L. Wagner, Andrea Wu¨ est, Ivan P. Christov, Tenio Popmintchev, Xibin Zhou, Margaret M. Murnane*, & and Henry C. Kapteyn. Monitoring molecular dynamics using coherent electrons from high harmonic generation. *PNAS* **103,** 13279–13285 (2006).

28. Perchard, J. P. Anharmonicity and hydrogen bonding. III. Analysis of the near infrared spectrum of water trapped in argon matrix. *Chem. Phys.* **273,** 217–233 (2001).

BIOGRAPHY

Originally from Springfield, VA, I moved to Lorton, VA and attended South County Secondary School. While there I had a great chemistry teacher who fostered my love of chemistry and science in general. I graduated in 2009 with an honors diploma as one of the top valedictorians in my class. I attended college at the University of Mary Washington in Fredericksburg, VA where I majored in chemistry and minored in mathematics. I graduated with honors from UMW in 2013 with a Bachelor of Science. I was then accepted into the chemistry Master's program at George Mason University.